TECHNICAL REPORT BRL-TR-3182

BRL

PROCESS-INDUCED STRESS AND DEFORMATION IN THICK-SECTION THERMOSET COMPOSITE LAMINATES

TRAVIS A. BOGETTI
JOHN W. GILLESPIE, JR.

DECEMBER 1990

U.S. ARMY LABORATORY COMMAND

BALLISTIC RESEARCH LABORATORY
ABERDEEN PROVING GROUND, MARYLAND

NOTICES

Destroy this report when it is no longer needed. DO NOT return it to the originator.

Additional copies of this report may be obtained from the National Technical Information Service, U.S. Department of Commerce, 5285 Port Royal Road, Springfield, VA 22161.

The findings of this report are not to be construed as an official Department of the Army position, unless so designated by other authorized documents.

The use of trade names or manufacturers' names in this report does not constitute indorsement of any commercial product.

REPORT DOCUMENTATION PAGE

Form Approved
OMB No. 0704-0188

1. AGENCY USE ONLY (Leave blank)	2. REPORT DATE	3. REPORT TYPE AND DATES COVERED
	DECEMBER 1990	Final, Jan 89 - Apr 90

4. TITLE AND SUBTITLE

Process-Induced Stress and Deformation in Thick-Section Thermoset Composite Laminates

5. FUNDING NUMBERS

PR: 1L1662618AH80

6. AUTHOR(S)

Travis A. Bogetti and John W. Gillespie, Jr.*

7. PERFORMING ORGANIZATION NAME(S) AND ADDRESS(ES)

8. PERFORMING ORGANIZATION REPORT NUMBER

9. SPONSORING/MONITORING AGENCY NAME(S) AND ADDRESS(ES)

US Army Ballistic Research Laboratory
ATTN: SLCBR-DD-T
Aberdeen Proving Ground, MD 21005-5066

10. SPONSORING/MONITORING AGENCY REPORT NUMBER

BRL-TR-3182

11. SUPPLEMENTARY NOTES

*John W. Gillespie is the Associate Director for the Center for Composite Materials and Associate Professor of Mechanical Engineering at the University of Delaware, Newark, DE 19716.

12a. DISTRIBUTION/AVAILABILITY STATEMENT

Approved for public release; distribution is unlimited.

12b. DISTRIBUTION CODE

13. ABSTRACT (Maximum 200 words)

A study of process-induced stress and deformation in thick-section thermosetting composite laminates is presented. A one-dimensional cure simulation analysis is coupled to an incremental laminated plate theory model to study the relationships between complex gradients in temperature and degree of cure, and process-induced residual stress and deformation during cure. Thermal expansion and cure shrinkage contribute to changes in material specific volume and represent important sources of internal loading included in the analysis. Temperature and degree of cure gradients that develop during the curing process represent fundamental mechanisms that contribute to stress development not considered in traditional residual stress analyses of laminated composites. Model predictions of cure dependent epoxy modulus and curvature in unsymmetric graphite/epoxy laminates are correlated with experimental data. The effects of processing history (autoclave temperature cure cycle), laminate thickness, resin cure shrinkage and laminate stacking sequence on the evolution of process-induced stress and deformation in thick-section glass/polyester and graphite/epoxy laminates during cure are studied. The magnitude of process-induced residual stress is sufficient to initiate transverse cracks and delaminations. The results clearly indicate that the mechanics and performance of thick-section thermoset laminates are strongly dependent on processing history.

14. SUBJECT TERMS	15. NUMBER OF PAGES
Thermoset Composites, Thick Laminates, Cure Simulation, Residual Stress, Process-Induced Stress, Laminated Plate Theory, Processing History, Chemical Shrinkage, Thermosetting Resins	60
	16. PRICE CODE

17. SECURITY CLASSIFICATION OF REPORT	18. SECURITY CLASSIFICATION OF THIS PAGE	19. SECURITY CLASSIFICATION OF ABSTRACT	20. LIMITATION OF ABSTRACT
UNCLASSIFIED	UNCLASSIFIED	UNCLASSIFIED	UL

INTENTIONALLY LEFT BLANK.

Contents

List of Figures

List of Tables

INTENTIONALLY LEFT BLANK.

Acknowledgements

This work was funded by the Army Research Office University Research Initiative Program. The authors are grateful for their financial support.

INTENTIONALLY LEFT BLANK.

1 Introduction

The development of residual stress is strongly influenced by processing history. Residual stresses can have a significant effect on the mechanical performance of composite structures by inducing warpage or initiating matrix cracks and delaminations [1,2,3,4]. Processing concerns associated with thermosetting composites become increasingly important for components of appreciable thickness. The most common problem is an increase in temperature resulting from the resin exothermic chemical reaction (polymerization) that may raise internal temperatures to levels inducing material degradation. A second concern is the complex gradients in temperature and degree of cure accentuated by increased thickness. This study focuses on the evolution of macroscopic in-plane residual stresses in thick thermoset laminates resulting from complex temperature and degree of cure gradients that develop during the curing process.

Traditional analyses of residual stresses in thermosetting composite laminates are based on thermal expansion mismatch between adjacent plies, a uniform temperature difference between the cure temperature and ambient and no stress development prior to completion of the curing process [3,4,5,6]. These analyses have been quite successful in predicting residual stresses in *thin* laminates, where a uniform through-the-thickness temperature distribution assumption is justified. Such an approach, however, is not appropriate for predicting the process-induced stresses in thick thermoset composite laminates where complex temperature and degree of cure gradients develop during the curing process [7,8,9,10,11,12,13]. As we demonstrate, these temperature and degree of cure gradients represent important mechanisms that contribute to the development of stress and deformation in thick-section composite laminates.

These mechanisms are quite similar to those which govern the development of residual stresses encountered in the manufacture of tempered glass [14,15,16,17]. Stresses result from the interactions between spatially varying thermal contractions and viscoelastic material response induced by severe temperature gradients which develop during the quenching process. Early treatment of this type of stress development due to viscoelastic material response in the presence of thermal gradients were based on the time-temperature superposition principle of rheologically simple material behavior [18].

This approach has been applied to study the macroscopic in-plane residual stress development under the rapid cooling process of an isotropic epoxy plate [19] and more recently to the quenching of thermoplastic matrix composite laminates [20].

Complex temperature and degree of cure gradients which develop in thick-section thermosetting laminates during the curing process induce spatially varying material response similar to that which induces viscoelastic stress development in rapid cooling and quenching processes. Birefringence patterns have shown the effect of temperature and degree of cure gradients on the development of residual stresses in thick thermoset castings [7]. In a series of papers, Levitsky and Shaffer [21,22,23] have studied the development of residual stresses including temperature gradients and spatially varying *chemical hardening* effects on mechanical properties in isotropic thermosetting materials accentuated by the exothermic chemical reaction. These studies indicate that temperature and degree of cure gradients significantly influence stress development prior to a fully cured state and consequently should be accounted for in studying the evolution of process-induced stress and deformation in thick-section thermosetting composite laminates.

Another important mechanism contributing to stress development not considered in the analyses cited [21,22,23] is the volumetric shrinkage of the thermosetting resin associated with the cross-link polymerization reaction. The importance of chemical shrinkage, which is an additional source of internal loading, can be appreciated by considering the shrinkage occurring within the interior region of a laminate that is constrained by a fully cured exterior region. A similar situation occurs on the micromechanics level where resin shrinkage during cure is constrained by the reinforcement phase [24].

As a thermosetting resin cures its material characteristics change dramatically, transitioning from the behavior of a viscous liquid (low stiffness), in its uncured state, to a viscoelastic or elastic solid (high stiffness), in its fully cured state. Significant reduction in specific volume (cure shrinkage) associated with the cross-link polymerization reaction also occurs during cure. These changes in the resin directly influence the effective mechanical properties and cure shrinkage strains of the composite during cure.

In the present investigation, the curing process of the resin is separated into three distinct

regions for descriptive purposes as shown in Figure 1. In Region I, the resin is in the B-stage condition, fully uncured and assumed to behave as a viscous fluid (negligible stiffness). Region II denotes the curing stage of the resin, where a significant increase in stiffness (chemical hardening) and a reduction in specific volume (chemical shrinkage) occurs. In this region the mechanical properties of the resin are governed inherently by competing mechanisms between chemical-kinetic hardening and viscoelastic relaxation phenomena. Region III marks the end of the curing process and no further chemical shrinkage occurs. In Region III the resin exhibits traditional viscoelastic behavior at elevated temperatures and approaches elastic behavior at lower temperatures. Thermal expansion is the only mechanism contributing to changes in specific volume in Region III.

This work focuses on the influence the curing process has on the macroscopic in-plane stress and deformation development in thick thermosetting composite laminates. A one-dimensional cure simulation model, based on an incremental transient finite difference formulation that accounts for thermal and chemical interactions, is developed to predict complex temperature and degree of cure gradients that develop during cure. Material models are proposed to describe the modulus and shrinkage of the resin during cure. Mechanical properties of the fiber phase are assumed independent of cure. A micromechanics model, employing the resin and fiber constituent behavior, is used to evaluate the instantaneous spatially varying mechanical properties, thermal expansion and chemical shrinkage strains within the composite laminate as a function of temperature and degree of cure. Process-induced stress and deformation predictions are based on an incremental laminated plate theory model that includes temperature gradients, spatially varying cure dependent mechanical properties, thermal expansion and chemical shrinkage strains. The incremental laminated plate theory model and cure simulation analysis are coupled enabling the prediction of macroscopic in-plane process-induced stress and deformation in thick composite laminates during the curing process to be made.

The methodology developed for predicting process-induced stress and deformation in thick sections is coded into a FORTRAN computer program. The program is employed in parametric studies to quantify the influence of processing on residual stress development in thick glass/polyester and graphite/epoxy thermoset laminates. Model predictions of cure dependent epoxy modulus

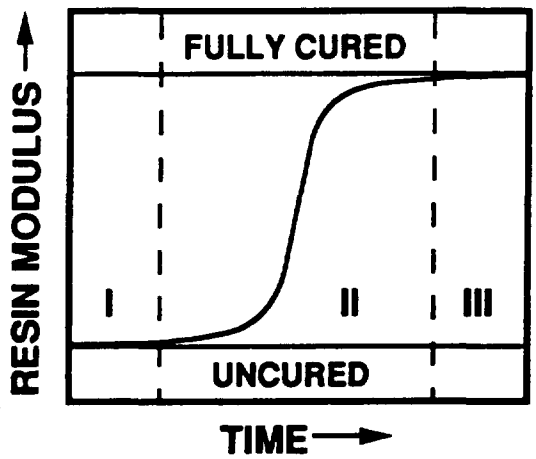

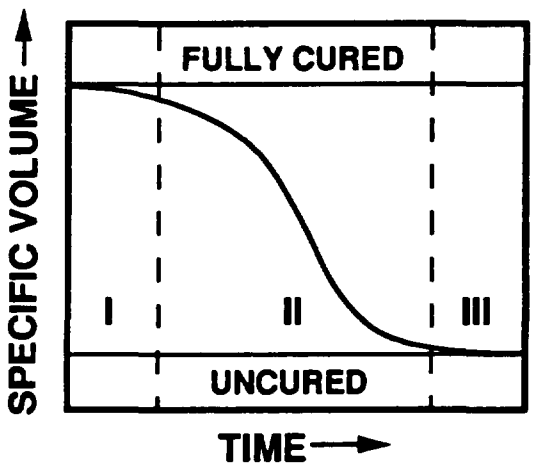

Figure 1: Resin modulus and chemical shrinkage during cure.

and curvature in unsymmetric graphite/epoxy laminates are correlated with experimental data. Processing history (autoclave temperature cycle), laminate thickness and resin cure shrinkage are shown to have a profound influence on the residual stress development in thick sections. The influence of unsymmetric curing (curing the laminate from one side) and laminate stacking sequence on process-induced stress development is also investigated. Results are presented which demonstrate that the traditional assumption of a stress-free laminate temperature is not generally appropriate for predicting residual stresses in thick themoset composite laminates.

2 Analysis

2.1 Cure Simulation

The one-dimensional cure simulation analysis presented herein was developed as a simplification of the authors' full two-dimensional anisotropic cure simulation analysis for complex shaped cross-sectional geometries [9,13]. A one-dimensional analysis enables isolation of through-the-thickness processing effects on a fundamental level without the extra computational effort required in a two-dimensional analysis. The solution strategy utilized in the cure simulation analysis is consistent with the treatment made by previous investigators [25,26]. The principle governing equation utilized in the analysis is the one-dimensional Fourier's Heat Conduction Equation:

$$\dot{q} + k_z \frac{\partial^2 T}{\partial z^2} = \rho c_p \frac{\partial T}{\partial t} \quad \text{for T(z,t) in } (0 < z < \ell) \tag{1}$$

The internal heat generation term, $\dot{q}$, accounts for the exothermic chemical reaction characteristic of thermosetting systems. The parameters k_z, ρ and c_p are the effective interlaminar (through-the-thickness) thermal conductivity, density and specific heat of the composite, respectively. These thermal properties are assumed constant during the curing process [7]. Total laminate thickness is ℓ. Absolute temperature and time are denoted T and t, respectively. The $z-$ direction is normal to the in-plane dimension of a laminate. Thermal properties for glass/polyester and graphite/epoxy used in this study are summarized in Table 1 [25,26,27].

A generalized temperature boundary condition formulation was employed allowing for either

	ρ [kg/m^3]	c_p [kJ/(W·°C)]	k_z [kW/(m · °C)]
Glass/Polyester	$1.89\text{x}10^3$	1.26	$2.163\text{x}10^{-4}$
Graphite/Epoxy	$1.52\text{x}10^3$	$9.42\text{x}10^{-1}$	$4.457\text{x}10^{-4}$

Table 1: Thermal properties for glass/polyester and graphite/epoxy.

convective, insulated or prescribed temperature boundary conditions on the laminate surface:

$$k_{eff}\frac{\partial T_s}{\partial z} + h_{eff}(T_s - T(t)) = 0$$
$$\text{at z} = 0 \text{ and z} = \ell \tag{2}$$

The temperature and normal derivative of temperature on the laminate surface are denoted T_s and $\partial T_s/\partial z$, respectively. The coefficients k_{eff} and h_{eff} represent the effective thermal conductivity and convective heat transfer coefficient on the laminate surface, respectively. The autoclave temperature cure cycle is incorporated into the cure simulation through $T(t)$. Prescribed temperature boundary conditions (k_{eff}=0 and h_{eff}=1) were employed in all simulations presented in this work to eliminate the added complexity of interpreting the influence of convection on the results [9,13].

The internal heat generation term in equation (1), $\dot{q}$, represents the instantaneous heat liberated per unit volume of material from the cross-link polymerization reaction:

$$\dot{q} = \rho H_r \frac{d\alpha}{dt} \tag{3}$$

The heat of reaction, H_r, is the total heat liberated for complete cure and $d\alpha/dt$ is the instantaneous cure rate. The degree of cure at any time is defined in terms of the instantaneous cure rate through an integral representation:

$$\alpha(t) = \int_0^t \frac{d\alpha}{dt} dt \tag{4}$$

The complete description of the cure kinetics for the composite includes the total heat of reaction and a description of the rate of reaction as a function of temperature and degree of cure. The instantaneous reaction rate is required to compute the heat generation (equation (3)) and degree of cure (equation (4)) during the curing process. Both the total heat of reaction and the reaction rate

expression are typically characterized empirically with isothermal Differential Scanning Calorimetry (DSC) techniques [27]. Reaction rate expressions for glass/polyester and graphite/epoxy are different in form due to the inherent differences in the overall order of the reaction kinetics.

The glass/polyester composite contains CYCOM 4102 polyester resin, manufactured by the American Cyanamid Corporation, and is reinforced with E-glass fibers (54% by volume). The reaction rate expression for glass/polyester is second-order overall in the sense that ($m_c + n_c = 2$), [27]:

$$\frac{d\alpha}{dt} = A_c exp(-\Delta E_c/RT)\alpha^{m_c}(1-\alpha)^{n_c} \tag{5}$$

The parameter R denotes the universal gas constant. The exponents m_c and n_c, the pre-exponential coefficient, A_c, the activation energy, ΔE_c, and the total heat of reaction, H_r, for glass/polyester are listed in Table 2.

The graphite/epoxy composite contains Hercules Corporation's 3501-6 epoxy resin and is reinforced with unidirectional AS4 graphite fibers (67% by volume). The reaction rate expression for graphite/epoxy follows a markedly different form [25,26]:

$$\frac{d\alpha}{dt} = (k_1 + k_2\alpha)(1-\alpha)(0.47-\alpha) \qquad \text{for} \quad (\alpha \leq 0.3)$$
$$\frac{d\alpha}{dt} = k_3(1-\alpha) \qquad \text{for} \quad (\alpha > 0.3) \tag{6}$$

The parameters k_1, k_2 and k_3 are defined by the Arrhenius rate expressions

$$\begin{aligned} k_1 &= A_1 exp(-\Delta E_1/RT) \\ k_2 &= A_2 exp(-\Delta E_2/RT) \\ k_3 &= A_3 exp(-\Delta E_3/RT) \end{aligned} \tag{7}$$

The pre-exponential coefficients A_1, A_2 and A_3, the activation energies, ΔE_1, ΔE_2 and ΔE_3, and the total heat of reaction for graphite/epoxy are summarized in Table 2 [25,26,27].

Initial conditions for temperature and degree of cure are mathematically represented by

$$\begin{aligned} T(z) &= T_i \text{ for } (0 \leq z \leq \ell) \text{ at t} = 0 \\ \alpha(z) &= \alpha_i \text{ for } (0 \leq z \leq \ell) \text{ at t} = 0 \end{aligned} \tag{8}$$

Glass/Polyester	
m_c	0.524
n_c	1.476
A_c[min.$^{-1}$]	3.7x10^{22}
ΔE_c[J/mol]	1.674x10^5
H_r[kJ/kg]	77.5
Graphite/Epoxy	
A_1[min.$^{-1}$]	2.102x10^9
A_2[min.$^{-1}$]	-2.014x10^9
A_3[min.$^{-1}$]	1.960x10^5
ΔE_1[J/mol]	8.07x10^4
ΔE_2[J/mol]	7.78x10^4
ΔE_3[J/mol]	5.66x10^4
H_r[kJ/kg]	198.9

Table 2: Cure kinetic parameters for glass/polyester and graphite/epoxy.

T_i and α_i are the prescribed uniform initial temperature and degree of cure distributions within the laminate taken to be the ambient temperature and zero, respectively.

An incremental transient finite difference technique is employed to solve the governing equations, boundary and initial conditions that define the cure simulation in question. Transient temperature and degree of cure distributions (through-the-thickness) are predicted as a function of the thermal properties, chemical-kinetic parameters, initial and boundary conditions including the autoclave temperature cure cycle. The laminate is discretized in the thickness dimension (z) with a one-dimensional finite difference nodal grid. The spatial and time derivatives in the governing temperature equation (1) and the boundary condition (2) are replaced by their appropriate finite difference approximations [9,13]. Transient temperature distributions are solved from the resulting set of finite difference equations using the Alternating Direction Explicit (ADE) Method [28]. Degree of cure distributions are computed from a finite sum approximation of the integral representation given by equation (4). The solution strategy of the cure simulation marches out the autoclave temperature cure cycle until its completion. In this manner, the transient temperature and degree of cure distributions within the laminate are generated as a function of the processing

history. Details of the solution strategy are documented elsewhere [9,13].

2.2 Material Models

Two material models are proposed to describe the behavior of the thermoset resin during cure. These models describe the mechanical property changes and volumetric cure (chemical) shrinkage associated with the cross-linked polymerization reaction. Property changes and cure shrinkage of the resin during cure directly influence the homogeneous mechanical properties and process-induced strains in the composite. This influence is quantified with a micromechanics model for unidirectional continuous fiber reinforced composites. Mechanical property and process-induced strain gradients through the laminate thickness represent important mechanisms contributing to macroscopic in-plane stress and deformation development during cure. The material models that describe the resin behavior during cure, coupling the cure simulation and stress analysis, are discussed below.

2.2.1 Cure Dependent Resin Modulus

The resin modulus model describes the mechanical properties of the resin during cure. The resin modulus is strongly cure dependent, influenced by the kinetic-viscoelastic interactions successfully modeled by Dillman and Seferis [29]. While their model was rigorous, independent evaluation of the kinetic and viscoelastic parameters required extensive data reduction procedures. In addition, model predictions outside the temperature range cover by Dillman and Seferis were not reliable. Consequently, a more convenient *α-mixing rule model* [30] is proposed here to describe the kinetic-viscoelastic behavior of the resin modulus during cure. The instantaneous isotropic resin modulus, denoted E_m, is expressed explicitly in term of degree of cure:

$$E_m = (1-\alpha)E_m^o + \alpha E_m^\infty + \gamma\alpha(1-\alpha)(E_m^\infty - E_m^o) \qquad (9)$$

$$\text{where } (-1 < \gamma < 1)$$

The parameters E_m^o and E_m^∞ are the assumed fully uncured (Region I) and fully cured (Region III) temperature dependent resin moduli, respectively. The term γ is introduced to quantify the competing mechanisms between stress relaxation and chemical hardening [29]. Increasing γ physi-

Property	Polyester	Epoxy
E_m^o [MPa]	2.757	3.447
E_m^∞ [MPa]	2.757×10^3	3.447×10^3
v_{sh}^T [%]	4-6	1-3

Table 3: Resin characteristics during cure.

cally corresponds to a more rapid increase in modulus at lower degree of cure before asymptotically approaching the fully cured modulus. Note that this model is extremely sensitive to the kinetics of the resin and, therefore, the non-isothermal process history (see equations (5) and (6)). Results presented in this study assume E_m^o and E_m^∞ are constant and $\gamma = 0$.

The instantaneous resin shear modulus during cure is based on the isotropic material relation:

$$G_m = \frac{E_m}{2(1+\nu_m)} \tag{10}$$

Poisson's ratio of the resin, ν_m, is assumed constant during cure. As this investigation focuses on the influence that the curing process has on stress and deformation development, all mechanical properties of the resin are assumed constant once cure is complete. Therefore, the analysis predictions for this assumption may provide upper bounds on process-induced stresses, since no stress relaxation is considered.

The fully uncured and fully cure resin moduli for glass/polyester and graphite/epoxy used in this study are listed in Table 3 [31]. Uncured moduli (E_m^o) are chosen arbitrarily small (*negligible* stiffness) while the fully cured moduli (E_m^∞) are representative of typical room temperature values.

In Figure 2, the model of Levitsky and Shaffer [21,22,23] is correlated with the present formulation for the chemical hardening of a polyester resin (see Tables 2 and 3) during isothermal cure at 100 °C. The present model assumes the Poisson ratio is constant while the latter model assumes the bulk modulus is constant. Both models predict nearly identical results for modulus development during cure. Deviation in Poisson ratio is noted at low degree of cure while the models converge rapidly as the resin cures (see Figure 2). The macroscopic composite properties, process-induced

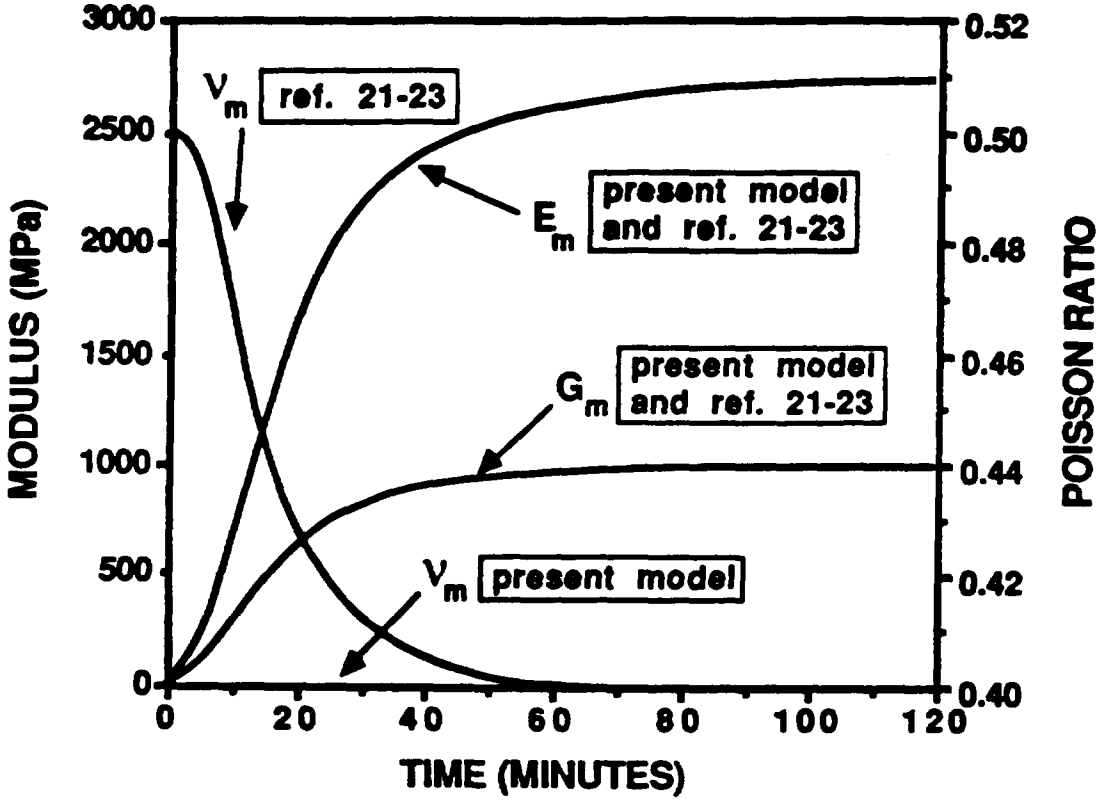

Figure 2: Influence of the constant poisson ratio assumption on modulus development during cure.

strains and residual stresses are not significantly influenced by this difference in the Poisson ratio of the resin during cure.

2.2.2 Cure Dependent Resin Chemical Shrinkage

A second material model is proposed to describe the volumetric chemical shrinkage of the resin during cure. Resin shrinkage only occurs during the curing process and ceases once cure is complete. Chemical resin shrinkage induces significant macroscopic strains in the composite, representing an important source of internal loading in thick-section laminates in addition to the traditionally recognized thermal expansion strains.

The volumetric change of a cubic volume element of dimension l_1 by l_2 by l_3 can be expressed in terms of its overall dimensions and the finite dimensional changes in three principle directions, Δl_1, Δl_2, Δl_3, as

$$\begin{aligned} \Delta V &= l_1 \Delta l_2 l_3 + \Delta l_1 l_2 l_3 + \Delta l_1 \Delta l_2 l_3 + l_1 l_2 \Delta l_3 + \\ & \quad l_1 \Delta l_2 \Delta l_3 + \Delta l_1 l_2 \Delta l_3 + \Delta l_1 \Delta l_2 \Delta l_3 \end{aligned} \tag{11}$$

An associated change in specific volume, Δv, can be defined in terms of the principle strain components,

$$\Delta v = \frac{\Delta V}{V} = \epsilon_1 + \epsilon_2 + \epsilon_3 + \epsilon_1\epsilon_2 + \epsilon_1\epsilon_3 + \epsilon_2\epsilon_3 + \epsilon_1\epsilon_2\epsilon_3 \tag{12}$$

Assuming a uniform strain contraction for all principle strain components, the incremental isotropic shrinkage strain, $\Delta\epsilon_r$, of a unit volume element of resin resulting from an incremental specific volume resin shrinkage, Δv_r, becomes[1]

$$\Delta\epsilon_r = \sqrt[3]{1 + \Delta v_r} - 1 \tag{13}$$

The incremental volume resin shrinkage is based on an incremental change in degree of cure, $\Delta\alpha$, and the total specific volume shrinkage of the completely cured resin, v_{sh}^T, through the following expression:

$$\Delta v_r = \Delta\alpha \cdot v_{sh}^T \tag{14}$$

[1]Exact expression suggested by Joseph M. Santiago, U.S. Army Ballistic Research Laboratory, Aberdeen Proving Ground, MD.

Typical total volumetric resin cure shrinkage values for glass/polyester and graphite/epoxy are listed in Table 3.

2.2.3 Cure Dependent Composite Mechanical Properties

The effective homogeneous unidirectional mechanical properties of each individual lamina within the composite laminate are computed each time increment during the cure simulation. Lamina properties are highly dependent on the fiber and resin constituent properties, and fiber volume fraction. The mechanical properties of the resin (except poisson ratio and thermal expansion which are assumed constant) vary according to the material models presented above. Mechanical properties of the fiber are assumed constant and independent of cure. During cure, significant composite property gradients develop as a result of the temperature and degree of cure gradients associated with thick laminate processing.

The doubly-embedded self-consistent field micromechanics model [32] is used to compute the instantaneous transversely isotropic mechanical properties and thermal expansion coefficients of the lamina. The micromechanics equations employed in this investigation are documented in the Appendix. The fiber and resin constituent mechanical properties for glass/polyester and graphite/epoxy are summarized in Table 4 [31]. The 1-direction is coincident with the direction of fiber reinforcement. The 2-direction (in-plane) and 3-direction (out-of-plane) are both perpendicular to the 1-direction. The graphite fiber is assumed transversely isotropic while the glass fiber is assumed isotropic. Note the strong resin property dependency on degree of cure and thus on the processing history.

2.2.4 Incremental Composite Chemical Shrinkage Strain

Effective chemical shrinkage strains in the composite are also computed according to the micromechanics model and are based on the fiber and resin mechanical properties, chemical resin shrinkage strain and fiber volume fraction. The in-plane principle lamina 1-direction (longitudinal) and 2-direction (transverse) chemical shrinkage strain increments, denoted $\Delta\epsilon_1^{ch}$ and $\Delta\epsilon_2^{ch}$, respectively,

Property	Glass	Polyester	Graphite	Epoxy
E_1 [MPa]	7.308×10^4	eqn.(10)	2.068×10^5	eqn.(10)
E_2 [MPa]	7.308×10^4	eqn.(10)	2.068×10^4	eqn.(10)
ν_{12}	0.22	0.40	0.20	0.35
ν_{13}	0.22	0.40	0.20	0.35
ν_{23}	0.22	0.40	0.50	0.35
G_{12} [MPa]	2.992×10^4	eqn.(10)	2.758×10^4	eqn.(10)
G_{13} [MPa]	2.992×10^4	eqn.(10)	2.758×10^4	eqn.(10)
G_{23} [MPa]	2.992×10^4	eqn.(10)	6.894×10^3	eqn.(10)
α_1 [1/°C]	5.04×10^{-6}	7.20×10^{-5}	-9.00×10^{-7}	5.76×10^{-5}
α_2 [1/°C]	5.04×10^{-6}	7.20×10^{-5}	7.20×10^{-6}	5.76×10^{-5}

Table 4: Fiber and resin constituent mechanical properties.

are computed over each time increment in the cure simulation. Specifically, these strains are based on the expansional strain relations of the micromechanics model utilizing the instantaneous mechanical properties of the fiber and resin, the resin chemical shrinkage strain increment, a zero stress-free shrinkage strain in the fiber and the fiber volume fraction.

2.2.5 Incremental Composite Thermal Expansion Strain

Incremental thermal expansion strains are also computed over each time increment during the cure simulation. They are based on the lamina temperature increment between two consecutive time steps, ΔT, and the instantaneous effective longitudinal and transverse thermal expansion coefficients, α_1 and α_2, respectively. The incremental longitudinal and transverse strain increments in each lamina are defined in the usual manner:

$$\Delta\epsilon_1^{th} = \alpha_1 \cdot \Delta T$$
$$\Delta\epsilon_2^{th} = \alpha_2 \cdot \Delta T \tag{15}$$

2.2.6 Total Incremental Composite Process-Induced Strain

The total stress-free macroscopic process-induced lamina strain increment (over a single time step) is computed by superimposing the thermal and chemical strain contributions. The total process-induced lamina strain increments in the longitudinal and transverse directions become

$$\Delta\epsilon_1^T = \Delta\epsilon_1^{th} + \Delta\epsilon_1^{ch}$$
$$\Delta\epsilon_2^T = \Delta\epsilon_2^{th} + \Delta\epsilon_2^{ch} \tag{16}$$

Both chemical (shrinkage) and thermal (expansional) strains are inherently elongational, consequently no shear strains in the principle material coordinate system are required in the analysis. Note, however, that process-induced shear strains will develop in the global laminate system when other than cross-ply [0/90] laminate constructions are considered.

2.3 Process-Induced Stress Modeling

Classical laminated plate theory forms the theoretical basis for the stress analysis presented herein [33, 34]. An incremental Hooke's law formulation is employed which utilizes the instantaneous effective composite properties and incremental process-induced lamina strain increments as input. Various incremental laminated plate theory solution strategies and convergence criteria are discussed elsewhere [35]. The theory and methodology employed in this study are discussed below.

Prior to the stress and deformation calculations for a single time step increment, the cure simulation is performed to yield the temperature and degree of cure distributions within the laminate. From these distributions, the instantaneous effective mechanical properties and incremental process-induced strains in the laminate are computed based on the material models discussed above. Stress and strain increments are then computed from the plate theory analysis over each time step in the cure simulation. This procedure is repeated for each time step increment of the cure simulation. By maintaining a cumulative sum of the stress and strain increments, a complete description of their transient development during the curing process and subsequent cool-down to uniform ambient temperature is obtained.

The laminate is discretized with nodal points in the z-direction, consistent with the finite difference grid employed in the cure simulation analysis. Mesh refinement is established such that a ply is defined between each pair of nodes in the finite difference grid, uniformly spaced a distance Δz. The temperature and degree of cure of a ply is taken as the arithmetic average of the cure simulation predicted values at the top and bottom nodes of that ply.

A fixed global laminate coordinate system is established where x- and y- are the in-plane directions and z- is the out-of-plane direction. The stress analysis presented here addresses macroscopic in-plane stress development induced by processing gradients in the out-of-plane direction. The principle (1, 2) coordinate system of each ply can be orientated any angle θ with respect to the fixed (x, y) global coordinate system of the laminate. Therefore, the analysis presented herein accommodates laminates of arbitrary stacking sequence.

The effective in-plane force and moment resultants are first calculated for the time step increment. The incremental in-plane force resultants, $\Delta N_x^T, \Delta N_y^T$ and ΔN_{xy}^T, and incremental moment resultants, $\Delta M_x^T, \Delta M_y^T$ and ΔM_{xy}^T, are given by:

$$\begin{aligned}
(\Delta N_x^T, \Delta M_x^T) &= \textstyle\sum_{k=1}^{N} (\bar{Q}_{11}^k \Delta\epsilon_x^T + \bar{Q}_{12}^k \Delta\epsilon_y^T + \bar{Q}_{16}^k \Delta\epsilon_{xy}^T)(1, z) \\
(\Delta N_y^T, \Delta M_y^T) &= \textstyle\sum_{k=1}^{N} (\bar{Q}_{12}^k \Delta\epsilon_x^T + \bar{Q}_{22}^k \Delta\epsilon_y^T + \bar{Q}_{26}^k \Delta\epsilon_{xy}^T)(1, z) \\
(\Delta N_{xy}^T, \Delta M_{xy}^T) &= \textstyle\sum_{k=1}^{N} (\bar{Q}_{16}^k \Delta\epsilon_x^T + \bar{Q}_{26}^k \Delta\epsilon_y^T + \bar{Q}_{66}^k \Delta\epsilon_{xy}^T)(1, z)
\end{aligned} \tag{17}$$

The total number of plies in the laminate is N. The matrix, $\bar{Q}_{ij}^k$, is the transformed plane stress stiffness matrix of the k^{th} ply defined in the global (x, y) laminate coordinate system in the traditional manner [33,34]:

$$\begin{aligned}
\bar{Q}_{11} &= m^4 Q_{11} + 2m^2 n^2 (Q_{12} + 2Q_{66}) + n^4 Q_{22} \\
\bar{Q}_{12} &= m^2 n^2 (Q_{11} + Q_{22} - 4Q_{66}) + (m^4 + n^4) Q_{12} \\
\bar{Q}_{22} &= n^4 Q_{11} + 2m^2 n^2 (Q_{12} + 2Q_{66}) + m^4 Q_{22} \\
\bar{Q}_{16} &= m^3 n (Q_{11} - Q_{12} - 2Q_{66}) + m n^3 (Q_{12} - Q_{22} + 2Q_{66}) \\
\bar{Q}_{26} &= m n^3 (Q_{11} - Q_{12} - 2Q_{66}) + m^3 n (Q_{12} - Q_{22} + 2Q_{66}) \\
\bar{Q}_{66} &= m^2 n^2 (Q_{11} + Q_{22} - 2Q_{12} - 2Q_{66}) + (m^4 + n^4) Q_{66}
\end{aligned} \tag{18}$$

where $m = cos\theta$ and $n = sin\theta$ and the nonzero stiffness constants in the principle material coordinate system are given by

$$\begin{aligned} Q_{11} &= \frac{E_1}{(1-\nu_{12}\nu_{21})} \\ Q_{12} &= \frac{E_1\nu_{21}}{(1-\nu_{12}\nu_{21})} \\ Q_{22} &= \frac{E_2}{(1-\nu_{12}\nu_{21})} \\ Q_{66} &= G_{12} \end{aligned} \tag{19}$$

The stress-free incremental ply strains, $\Delta\epsilon_x^T$, $\Delta\epsilon_y^T$ and $\Delta\epsilon_{xy}^T$, defined in the global laminate coordinate system, are based on the incremental stress-free process-induced ply strains in the principle lamina coordinate system (equation 16) through the second-order tensoral transformation

$$\begin{Bmatrix} \Delta\epsilon_x^T \\ \Delta\epsilon_y^T \\ \Delta\epsilon_{xy}^T \end{Bmatrix} = \begin{bmatrix} m^2 & n^2 & mn \\ n^2 & m^2 & -mn \\ -2mn & 2mn & (m^2-n^2) \end{bmatrix} \begin{Bmatrix} \Delta\epsilon_1^T \\ \Delta\epsilon_2^T \\ 0 \end{Bmatrix} \tag{20}$$

The effective incremental laminate in-plane strains, $\Delta\epsilon_x^o, \Delta\epsilon_y^o$ and $\Delta\epsilon_{xy}^o$, and curvatures, $\Delta\kappa_x$, $\Delta\kappa_y$ and $\Delta\kappa_{xy}$ are then evaluated:

$$\begin{Bmatrix} \Delta\epsilon_x^o \\ \Delta\epsilon_y^o \\ \Delta\epsilon_{xy}^o \\ \Delta\kappa_x \\ \Delta\kappa_y \\ \Delta\kappa_{xy} \end{Bmatrix} = \begin{bmatrix} a_{11} & a_{12} & a_{16} & b_{11} & b_{12} & b_{16} \\ a_{12} & a_{22} & a_{26} & b_{12} & b_{22} & b_{26} \\ a_{16} & a_{26} & a_{66} & b_{16} & b_{26} & b_{66} \\ b_{11} & b_{12} & b_{16} & d_{11} & d_{12} & d_{16} \\ b_{12} & b_{22} & b_{26} & d_{12} & d_{22} & d_{26} \\ b_{16} & b_{26} & b_{66} & d_{16} & d_{26} & d_{66} \end{bmatrix} \begin{Bmatrix} \Delta N_x^T \\ \Delta N_y^T \\ \Delta N_{xy}^T \\ \Delta M_x^T \\ \Delta M_y^T \\ \Delta M_{xy}^T \end{Bmatrix} \tag{21}$$

The matrices $[a_{ij}]$, $[b_{ij}]$ and $[d_{ij}]$ are the instantaneous effective laminate compliance coefficients computed in the traditional manner [33,34] with spatial variation of instantaneous mechanical ply properties taken into account.

Once the incremental in-plane strains and curvatures are determined, the laminate ply strain increments, $\Delta\epsilon_x$, $\Delta\epsilon_y$ and $\Delta\epsilon_{xy}$ are computed through the classic strain-displacement relations [33, 34]:

$$\begin{aligned} \Delta\epsilon_x &= \Delta\epsilon_x^o + z_k\Delta\kappa_x \\ \Delta\epsilon_y &= \Delta\epsilon_y^o + z_k\Delta\kappa_y \\ \Delta\epsilon_{xy} &= \Delta\epsilon_{xy}^o + z_k\Delta\kappa_{xy} \end{aligned} \tag{22}$$

Here z_k is the distance from the laminate mid-plane to the center of the k^{th} ply.

The incremental ply stresses are based on the difference between the laminate ply strain increments and the stress-free process-induced ply strain increments through the following expression:

$$\begin{aligned}
\Delta\sigma_x^k &= \bar{Q}_{11}^k(\Delta\epsilon_x - \Delta\epsilon_x^T)^k + \bar{Q}_{12}^k(\Delta\epsilon_y - \Delta\epsilon_y^T)^k + \bar{Q}_{16}^k(\Delta\epsilon_{xy} - \Delta\epsilon_{xy}^T)^k \\
\Delta\sigma_y^k &= \bar{Q}_{12}^k(\Delta\epsilon_x - \Delta\epsilon_x^T)^k + \bar{Q}_{22}^k(\Delta\epsilon_y - \Delta\epsilon_y^T)^k + \bar{Q}_{26}^k(\Delta\epsilon_{xy} - \Delta\epsilon_{xy}^T)^k \\
\Delta\sigma_{xy}^k &= \bar{Q}_{16}^k(\Delta\epsilon_x - \Delta\epsilon_x^T)^k + \bar{Q}_{26}^k(\Delta\epsilon_y - \Delta\epsilon_y^T)^k + \bar{Q}_{66}^k(\Delta\epsilon_{xy} - \Delta\epsilon_{xy}^T)^k
\end{aligned} \tag{23}$$

Transient process-induced stress and strain distributions through the laminate thickness are obtained from the cumulative sum of the increments computed at each time step during the cure simulation. The governing equations for the cure simulation, material models and stress analysis were coded into a FORTRAN computer program. A flow diagram summarizing the key steps in the solution strategy is presented in Figure 3. As an example of the computational efficiency of the computer simulation, a 2.54 cm thick laminate cured for six hours, consisting of 30 nodes and 10000 time steps, takes approximately two hours of CPU time. Parametric studies were performed to gain fundamental insight into process-induced stress development in thick-section thermoset laminates. Results are presented and discussed in the next section.

3 Results and Discussion

In this section input for the process-induced stress model is first summarized. Predictions of the effective composite in-plane modulus and process-induced strain development, associated with the cure reaction of the resin, are presented. Several aspects of the analysis are then validated by comparison with experimental results of modulus and laminate curvature found in previously published literature. Parametric studies are presented that focus on the effects of the autoclave temperature cure cycle, laminate thickness, stacking sequence, and resin cure shrinkage on process-induced stress and deformation development.

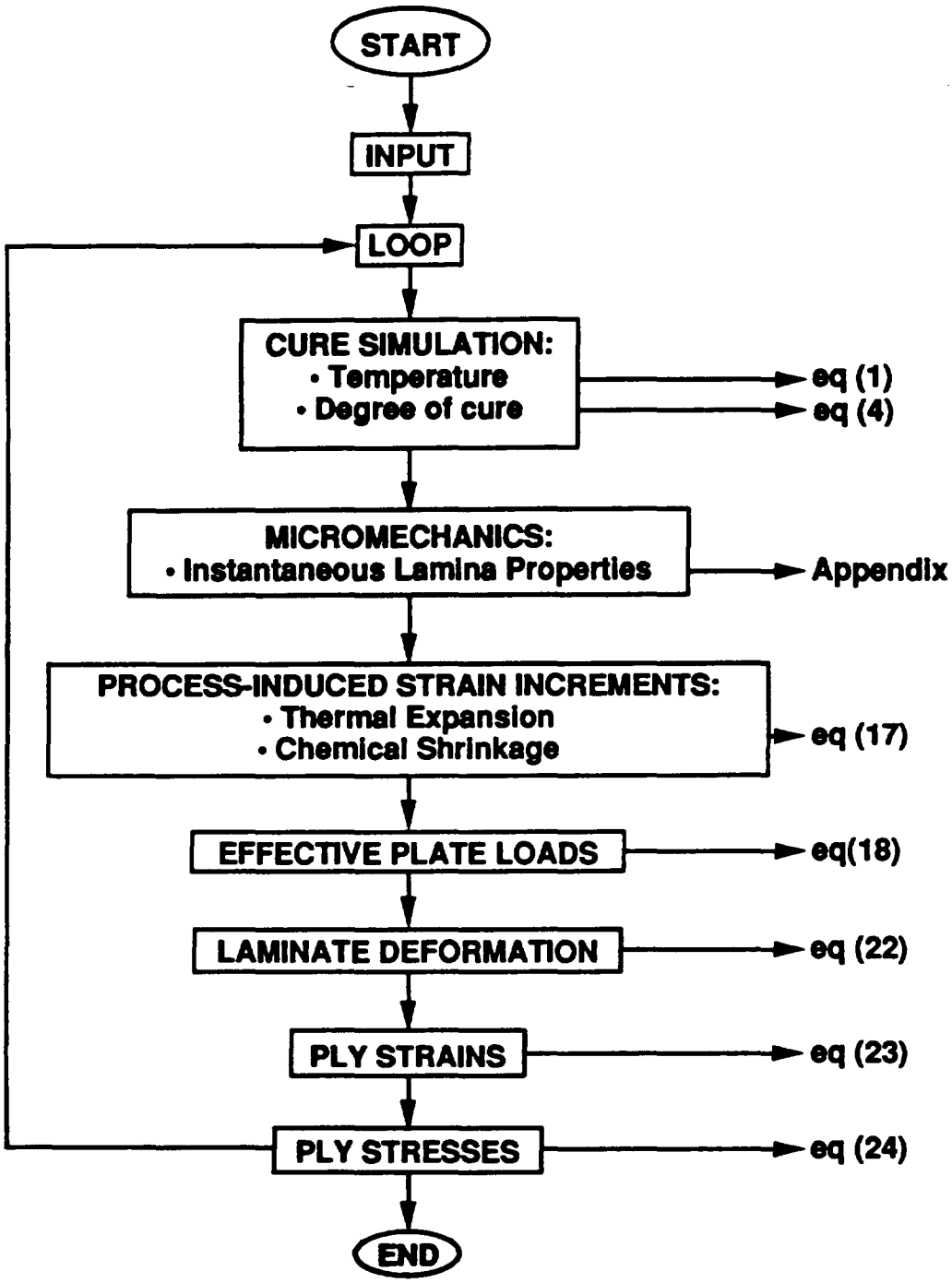

Figure 3: Process-induced stress modeling flow diagram.

3.1 Input Parameter Summary

Required model input includes thermal properties, kinetic parameters and mechanical properties. This input for glass/polyester and graphite/epoxy was summarized in Tables 1 through 4 in the previous section. Typical autoclave temperature cure cycles for glass/polyester and graphite/epoxy employed in the many of the parametric studies presented in this work are illustrated in Figure 4. Additional input (specified where appropriate) includes; total laminate thickness, stacking sequence and volumetric resin shrinkage.

As with all numerical solution techniques, the potential for computational round-off error exists. Convergence studies were conducted to evaluate the sensitivity of the analysis to nodal spacing and time step size increment. A nodal spacing of 2.30×10^{-3} m and a time step of 1.0 second were found to yield converged solutions for laminates up to 7.62 cm thick and were used to generate all results presented in this investigation.

3.2 Composite Behavior During Cure

3.2.1 Modulus

The influence of resin modulus on the effective composite properties during cure is quantified through the micromechanics model. Effective transverse and in-plane shear moduli of glass/polyester are presented in Figure 5 under isothermal cure at 100°C. The rapid increase in instantaneous moduli is indicative of the rapid curing. Gradients in this type of material response represent a significant mechanism for inducing stress in thick-section thermosetting laminates during the curing process.

3.2.2 Process-Induced Strains

Volumetric shrinkage of the resin is occurring simultaneously with effective mechanical property stiffening effects. Micromechanics predictions of the effective macroscopic composite chemical shrinkage strain account for the combined influence of the volumetric resin shrinkage and instan-

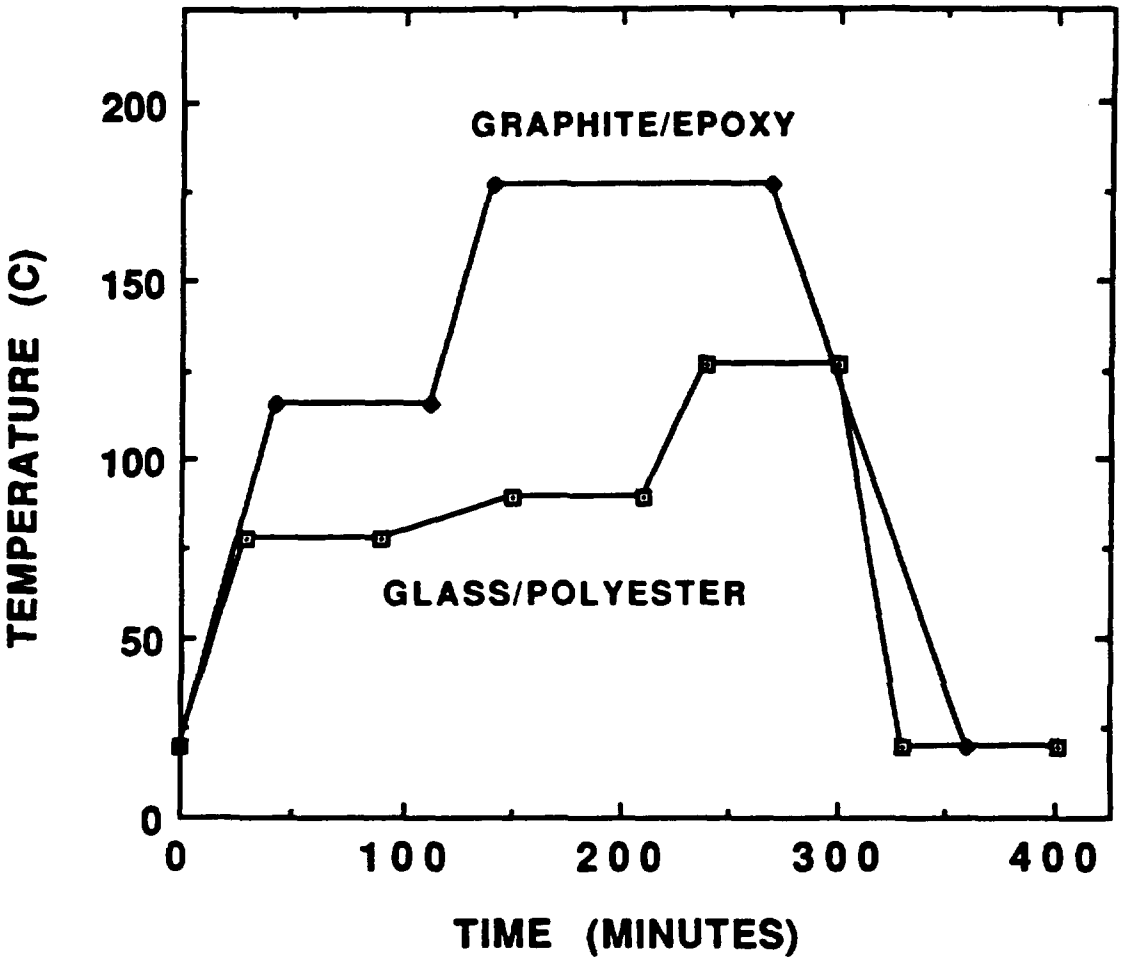

Figure 4: Typical autoclave cure cycles for glass/polyester and graphite/epoxy.

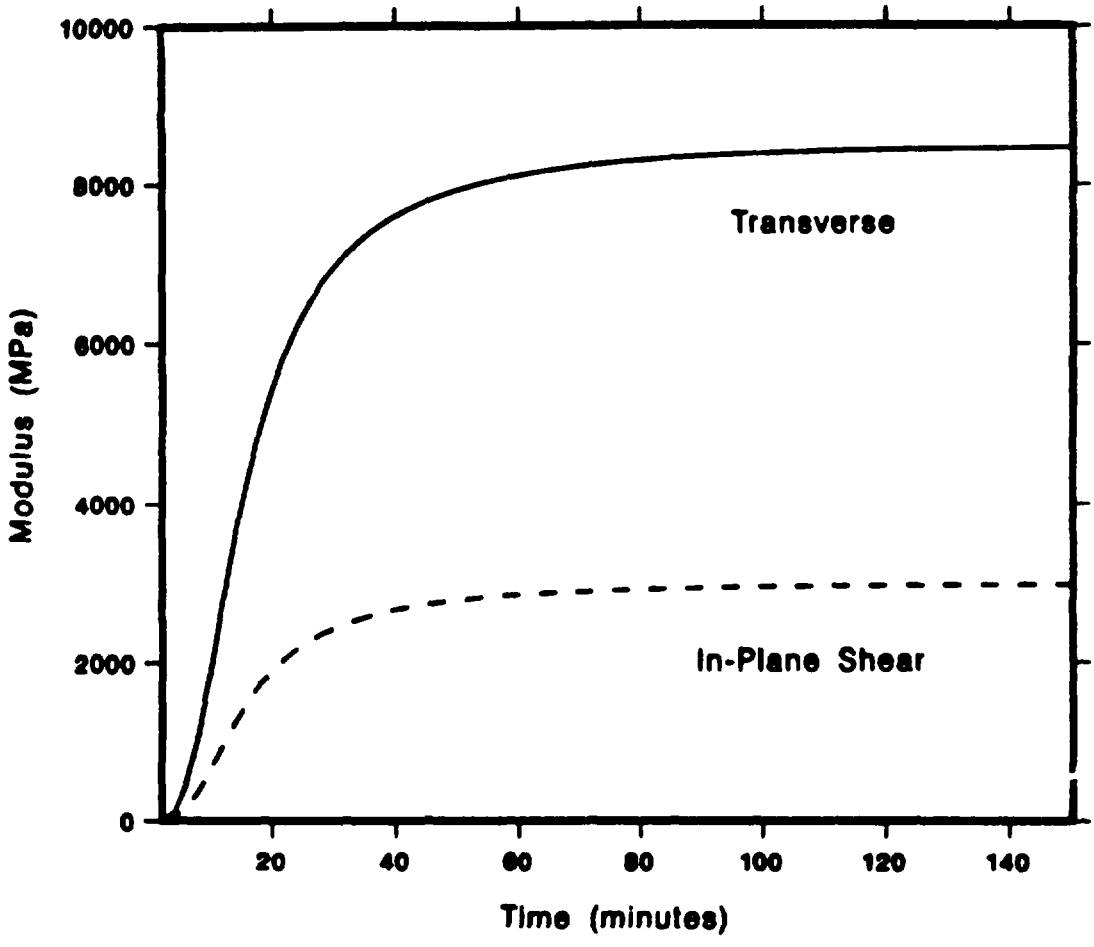

Figure 5: Glass/polyester moduli during isothermal cure at 100 °C.

taneous resin properties. The shrinkage strain in glass/polyester under isothermal cure at 100°C is illustrated in Figure 6 for a total volumetric resin shrinkage of v_{sh}^{T}=6%. While the longitudinal component is small, due to the constraining fiber stiffness, the effective transverse component is significant, exceeding 1%. Gradients in these shrinkage strains also represent a significant source for stress development not recognized in traditional residual stress analyses.

3.3 Comparison With Experimental Results

Hahn and Kim subjected several graphite/epoxy (T300/3501-6) unidirectional and [0/90] unsymmetric laminates to interrupted cure cycles to monitor the development of transverse modulus (in the unidirectional laminates) and curvature induced by cure shrinkage and thermal strains (in the unsymmetric laminates) [36]. Laminates were approximately 1 mm in thickness and the cure cycles followed the manufacturer's recommended cure cycle (see Figure 4). At each of a series of points during cure, a unidirectional and a cross-ply laminate were cooled to room temperature at 3°C/min. The unidirectional laminates were tensile tested to determine the transverse modulus, and the deflections of the unsymmetric laminates were measured to determine process-induced curvatures. Figure 7 shows excellent agreement between the measured and predicted transverse modulus development based on the material model presented herein. Note that the horizontal axis refers to time of cure stop. This indicates the time at which the cure cycle was interrupted and cooling to room temperature initiated, and does not indicate the time of the full cycle to which the laminate was subjected as not all laminates were cooled from the same temperature.

Figure 8 shows the development of non-dimensionalized curvature (with respect to laminate thickness) as a function of the time of cure stop for total epoxy resin volumetric shrinkages of 1.0 and 1.5 %. Again we see good agreement between measured and predicted values. Significant over-prediction of the curvature early in the cycle is thought to arise from the fact that the highly viscoelastic behavior of the resin, which has not yet reached gelation, is not incorporated in the present model. Also, the fracture surfaces of the tensile tested specimens in the region of the curvature over-prediction exhibited little or no interfacial bonding between the fibers and the resin, leading to a relatively unconstrained resin and reduced stress development. By defining the gel

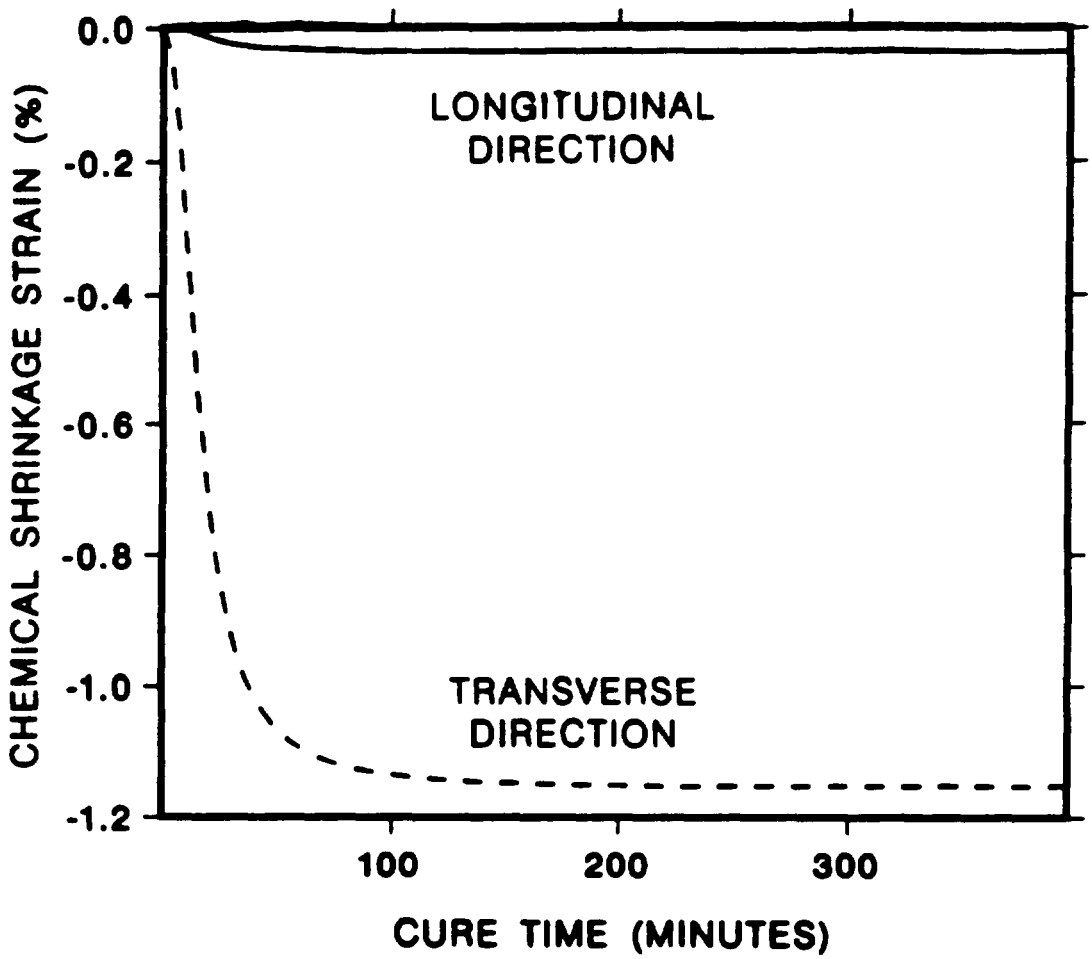

Figure 6: Glass/polyester chemical shrinkage strain during isothermal cure at 100 °C.

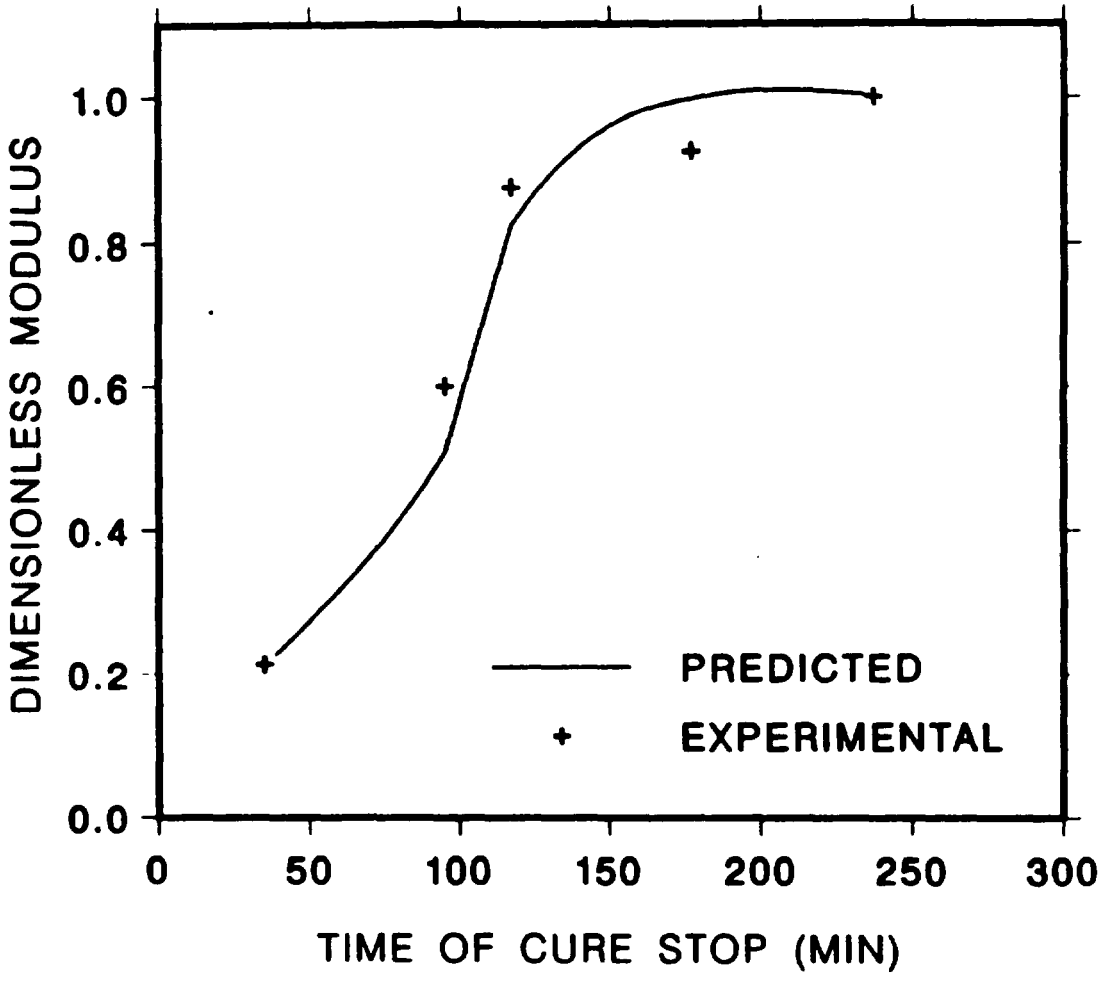

Figure 7: Experimental vs predicted composite transverse modulus development in a unidirectional graphite/epoxy laminate.

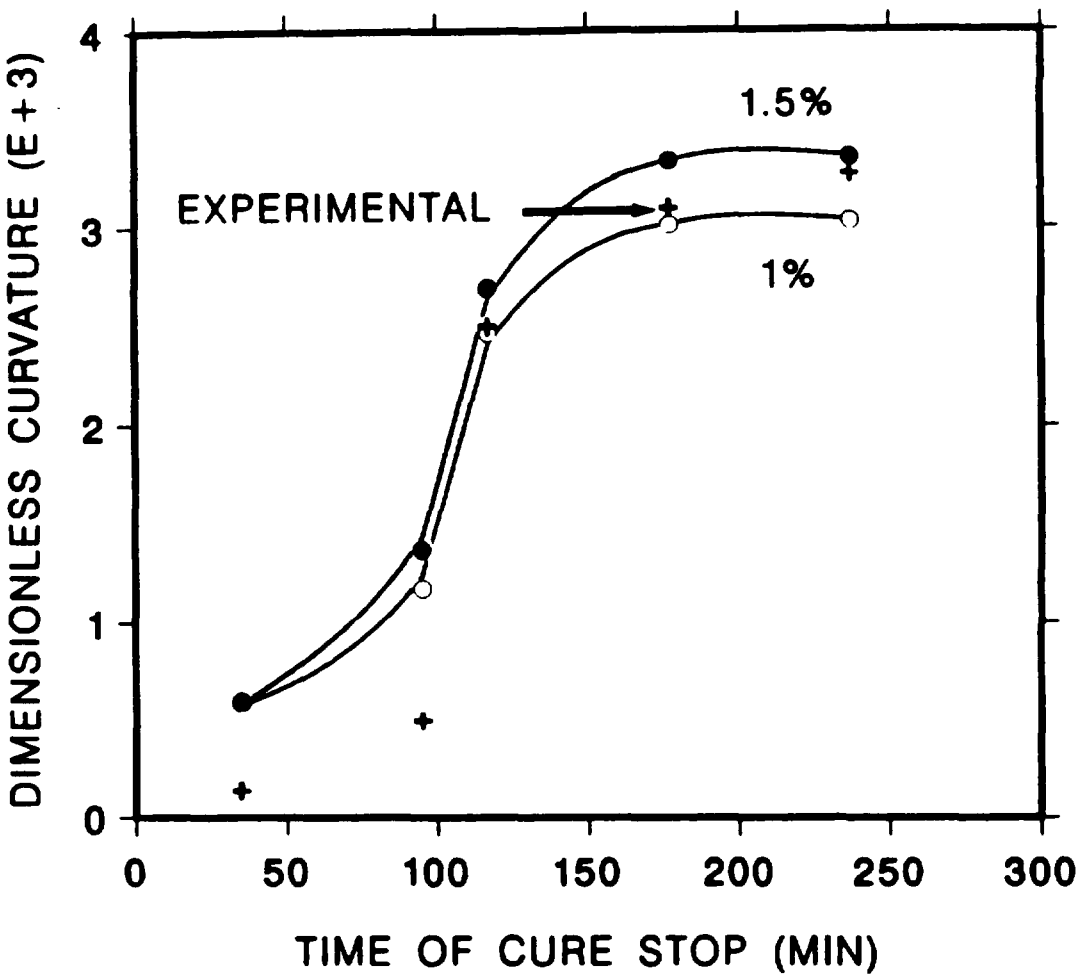

Figure 8: Experimental vs predicted curvature during cure of an unsymmetric [90/0] graphite/epoxy laminate.

point as the point at which the viscosity of the resin reaches 100 Pa-Sec, Hahn and Kim note that the curvature and the transverse modulus both increase sharply immediately after the gel point, possibly indicating that the development of residual stress can be significantly affected by the mechanical properties of the resin before full cure has been reached. Good agreement with the experimental results provides confidence in the accuracy of the analysis for predicting stress development during the curing process.

3.4 Thickness Effects

To gain an appreciation for the mechanisms introduced in this investigation, complex temperature and degree of cure distributions are illustrated in glass/polyester laminates of varying thickness exposed to the same cure cycle. The glass/polyester cure cycle, indicated in Figure 4, yields a maximum temperature exotherm in a 2.54 cm thick laminate at 164 minutes. Figure 9 illustrates the influence of laminate thickness on temperature distributions at 164 minutes into this cure cycle. Temperature exotherm increases with laminate thickness below 2.54 cm while the 5.08 cm laminate is still heating. Corresponding degree of cure distributions are illustrated in Figure 10. Degree of cure gradients are most severe at this point in the 2.54 cm laminate. The interior of the 2.54 cm laminate is essentially cured. In contrast, the 5.08 cm laminate is essentially uncured at the interior. At a later point in the cure cycle, the thicker laminate will exotherm and its distributions will reverse shape similar to the thinner laminates, ultimately developing more severe gradients. These results demonstrate the complex temperature and degree of cure gradients which develop during the curing process of thick thermoset laminates. These gradients in turn have a profound influence on the evolution process-induced stress and deformation.

Residual process-induced transverse stress distributions in 1.38, 1.85 and 2.54 cm thick unidirectional glass/polyester laminates were predicted for the cure cycle shown in Figure 4 with v_{sh}^{T}=6%. The results are presented in Figure 11. These significant stress distributions remain after complete cure and uniform ambient temperature conditions within the laminate exist. The parabolic stress profiles are self-equilibrating tensile stresses at exterior and compressive stresses at the interior regions. This profile is unique to laminates that cure predominantly from the inside to the outside

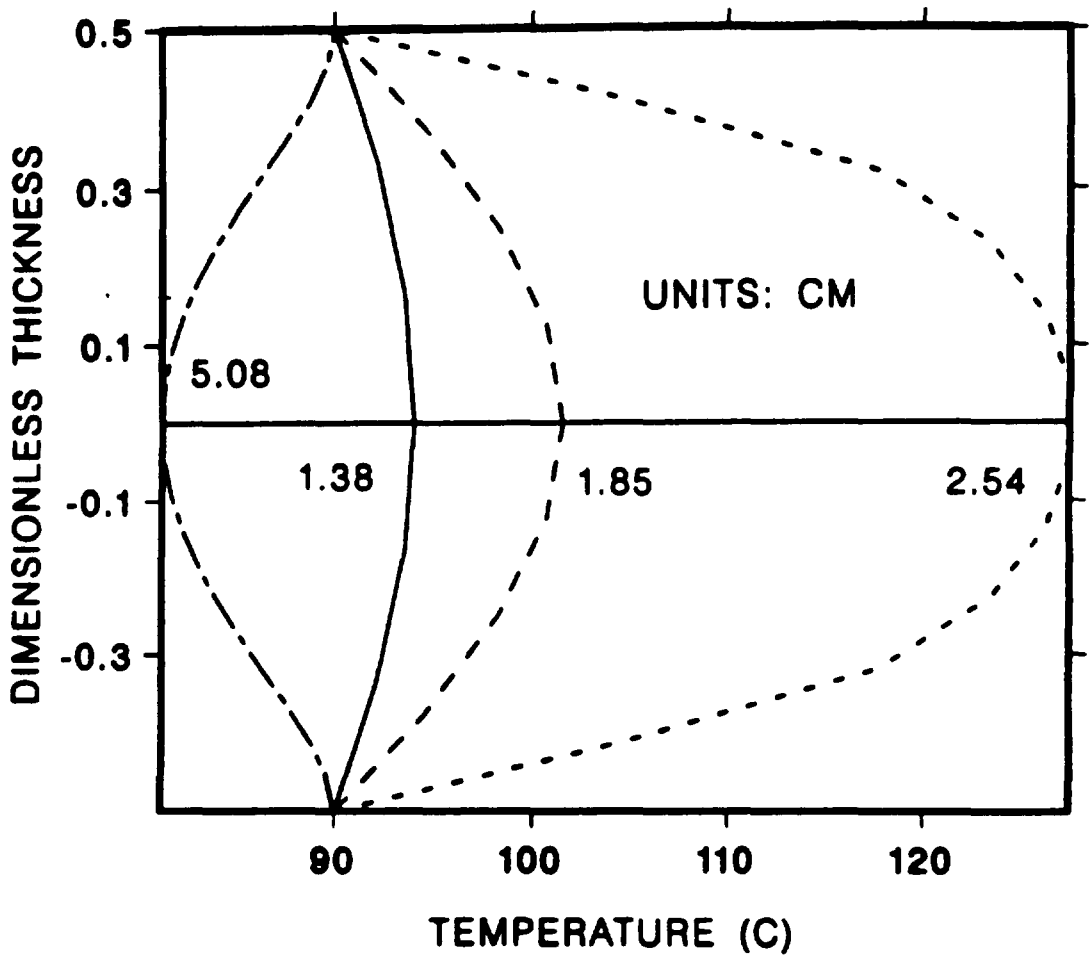

Figure 9: Temperature distributions in glass/polyester laminates at 164 minutes.

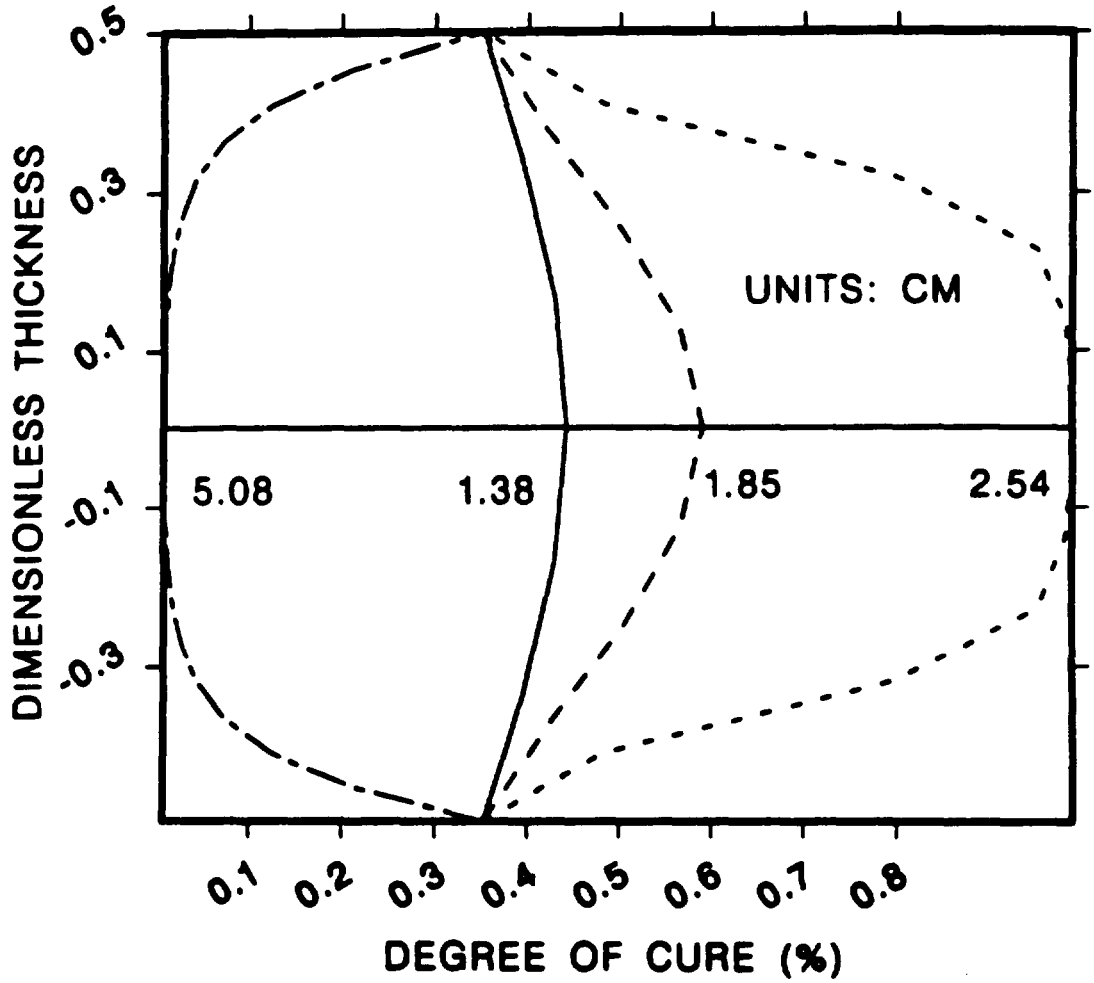

Figure 10: Degree of cure distributions in glass/polyester laminates at 164 minutes.

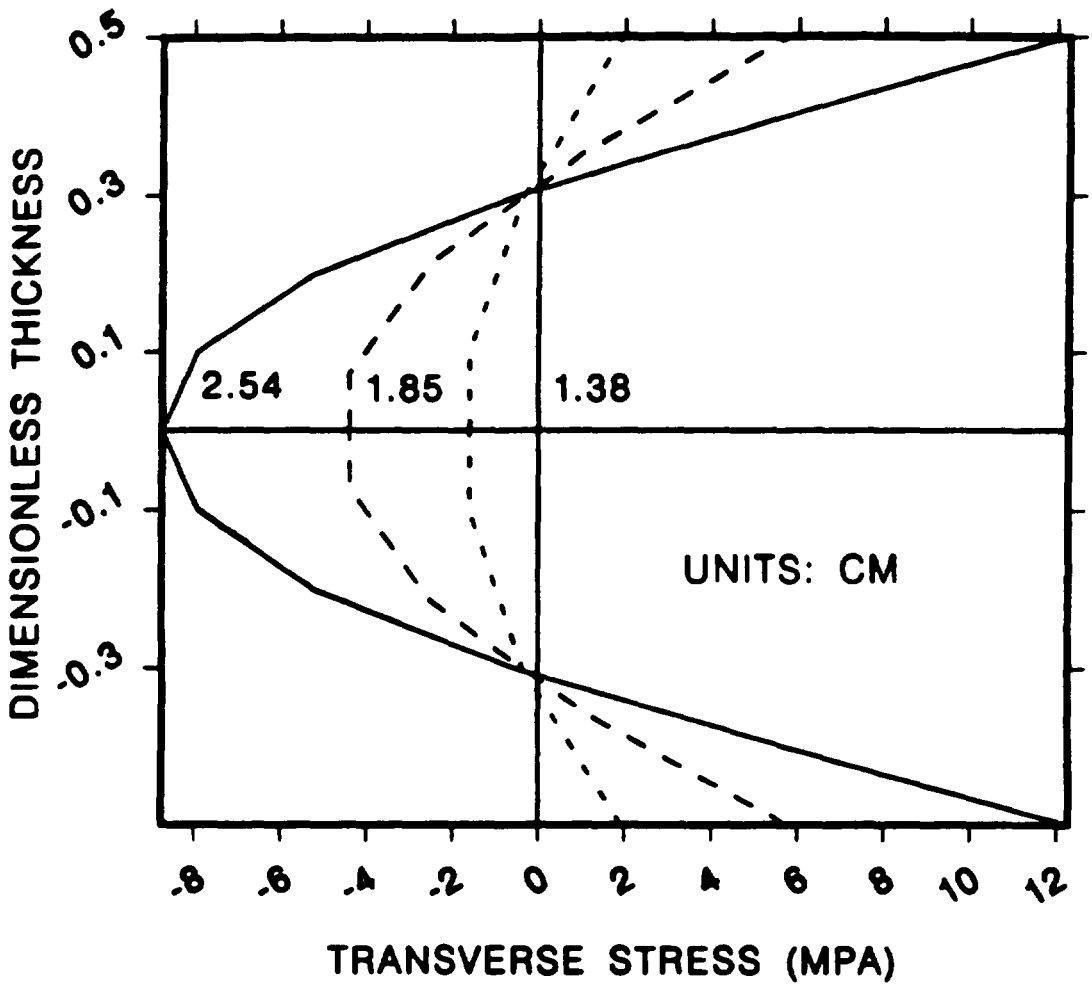

Figure 11: Residual process-induced in-plane transverse stress distributions ($\ell \leq 2.54$ cm).

surface of the part. Interior regions curing first, due to the exotherm, are less constrained by the uncured exterior region during shrinkage. As the exterior cures and contracts, it is constrained by the cured interior region of appreciable stiffness and the process-induced residual stresses shown in Figure 11 develop. Stress gradients are accentuated with increasing laminate thickness. For comparison purposes, it is pointed out that stress analyses based upon the traditional sources of residual stress associated with laminate stacking sequence predict that unidirectional laminates are stress free. This is clearly not the case with thick laminates.

Residual process-induced transverse stress distributions in unidirectional glass/polyester laminates 2.54, 5.08 and 7.62 cm thick, utilizing the same cure cycle and resin shrinkage, are illustrated in Figure 12. A dramatic parabolic stress reversal of the distributions in the 5.08 and 7.62 cm laminates are predicted where the interior regions are in tension and the exterior regions are in compression. This reversal results from the change to an outside to inside cure history in the thicker laminates and clearly demonstrates the significant influence the laminate thickness has on the evolution of process-induced stress. The magnitude of peak stresses and gradients which develop are significant enough to initiate transverse cracks [3,4,5,6].

3.5 Autoclave Temperature Cure Cycle Effects

The influence of the autoclave temperature cure cycle history on stress development is investigated by considering the curing of a unidirectional 2.54 cm glass/polyester laminate exposed to the temperature histories illustrated in Figure 13 and a resin shrinkage of v_{sh}^{T}=6 %. Resulting residual process-induced transverse stress distributions for temperature ramps of 0.25, 0.5 and 1.0 (°C/minute) are presented in Figure 14. The stress distributions developing under the temperature ramps of 0.25, 0.5 and 1.0 (°C/minute) induce compressive stresses at the interior, while the more rapid curing process results in the development of tensile interior stresses. These results demonstrate the importance of the processing history on residual stress development in thick laminates. The slower thermal ramps create an inside to outside cure history and consequently develop internal compressive stresses. As the ramp is increased the cure history changes to an outside to inside cure, resulting in a reverse in the parabolic stress distribution.

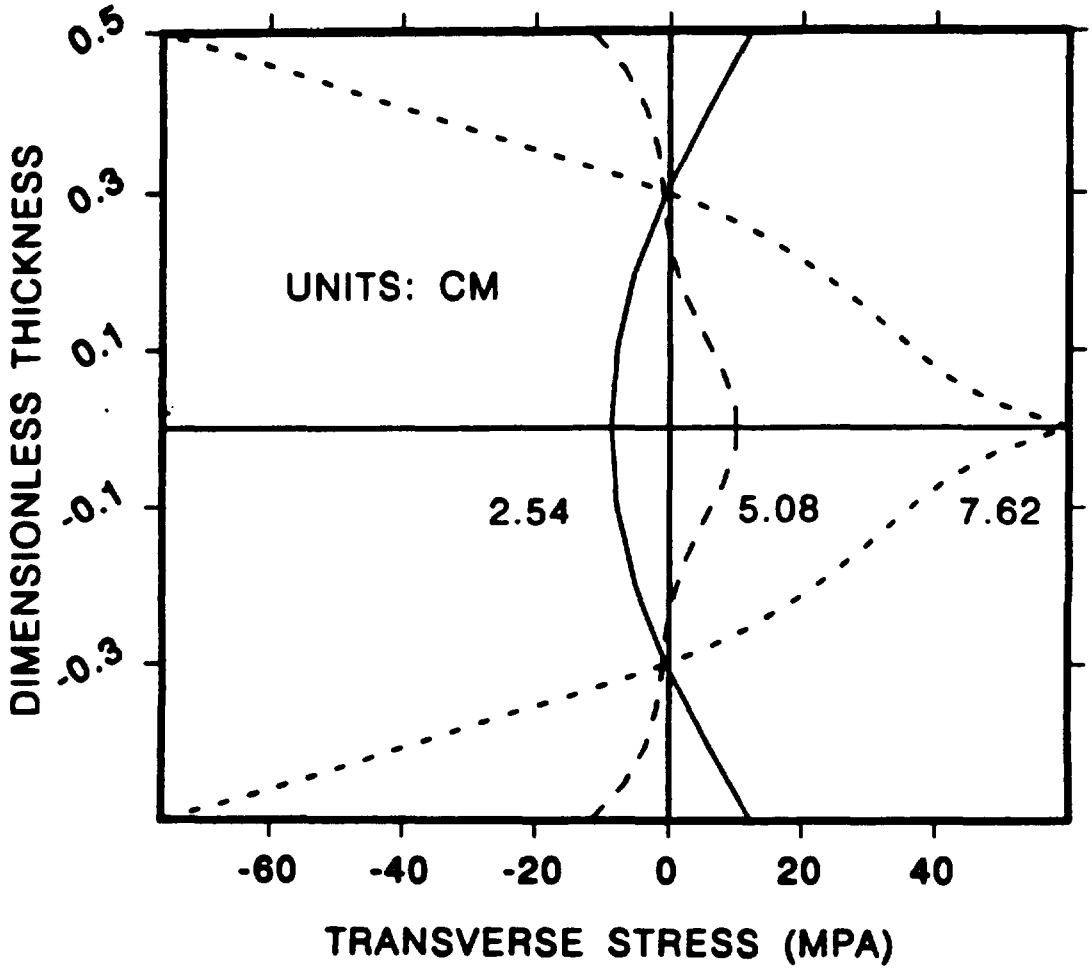

Figure 12: Residual process-induced in-plane transverse stress distributions ($\ell \geq 2.54$ cm).

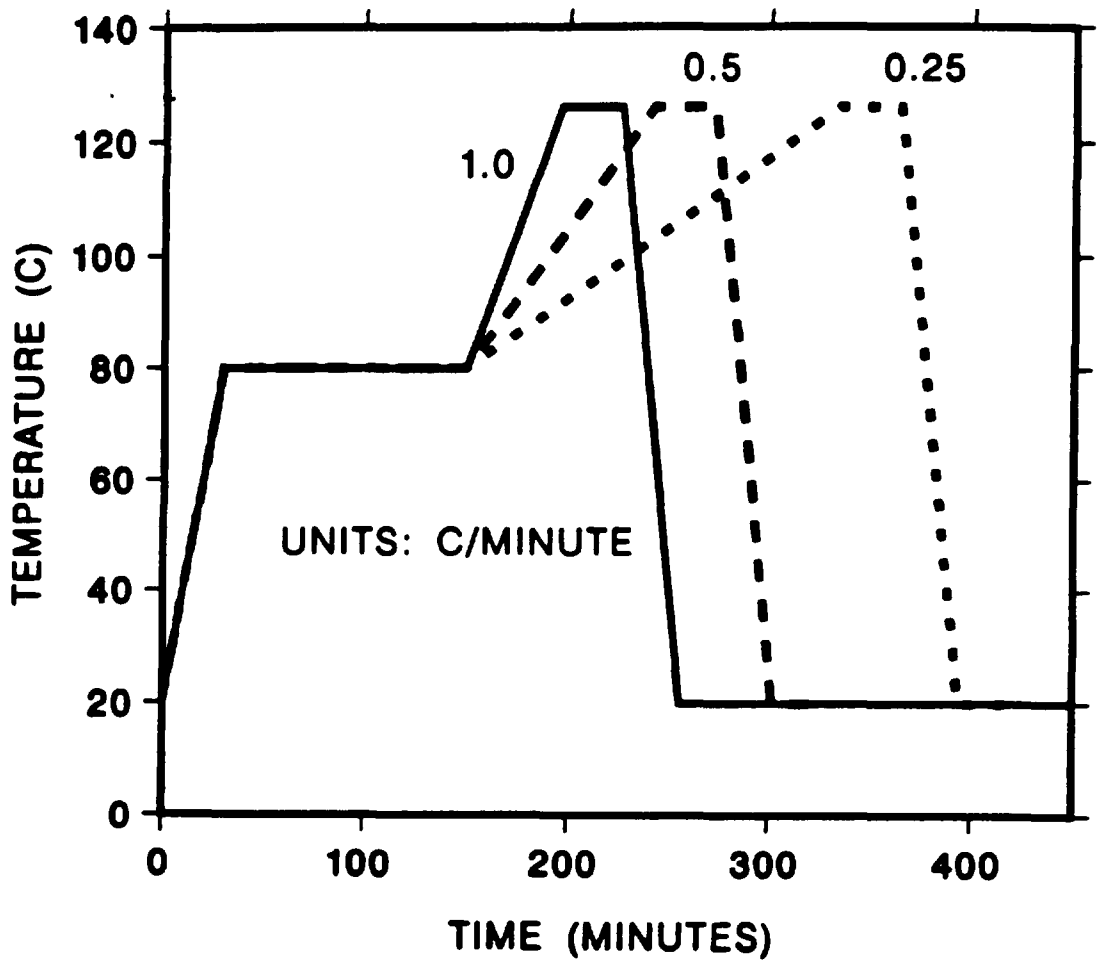

Figure 13: Glass/polyester autoclave temperature cure cycle ramps.

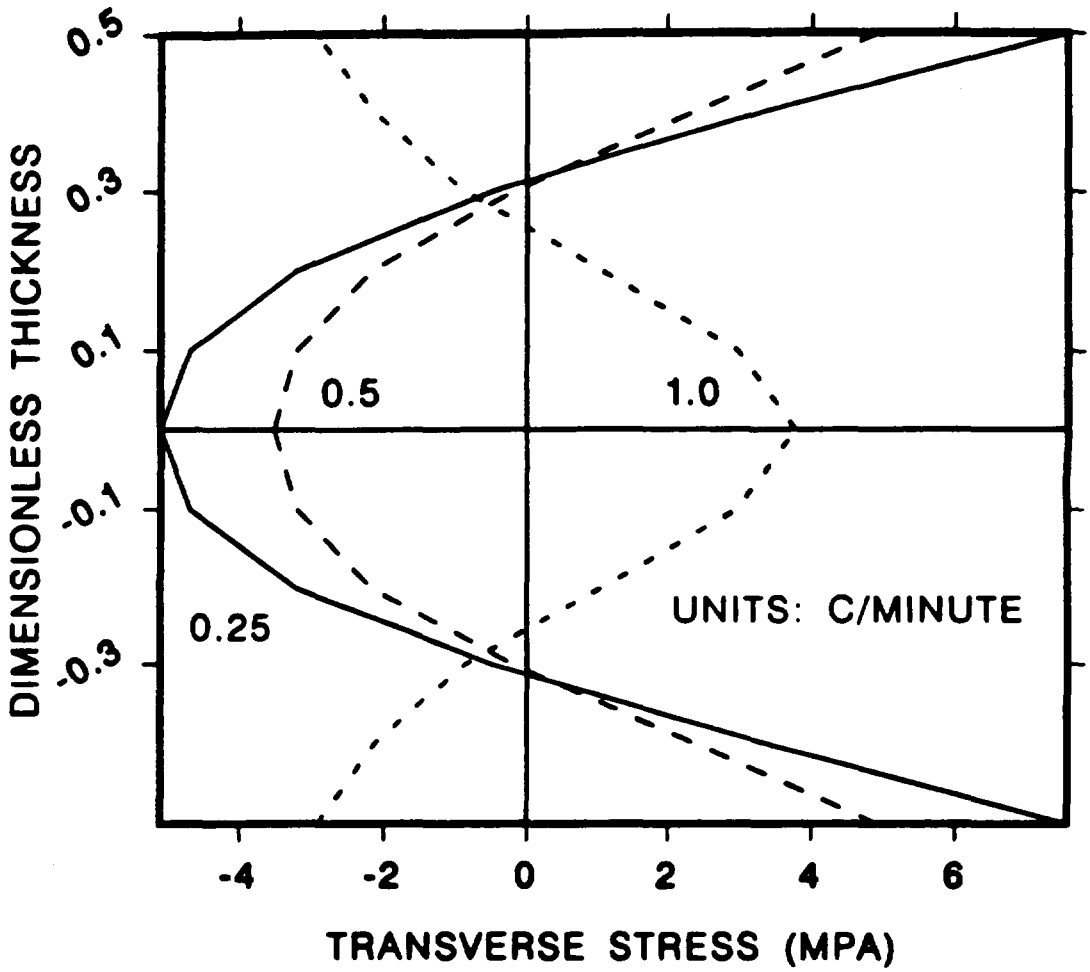

Figure 14: Glass/polyester autoclave temperature cure cycle ramp effects on transverse stress distributions ($\ell = 2.54$ cm).

3.6 Cure Shrinkage Effects

The influence of resin shrinkage on residual stress development was also investigated. Total volumetric resin shrinkages, v_{sh}^T, of 0, 1, 3 and 6 % are assumed in the simulations of a 2.54 cm unidirectional glass/polyester laminate cured according to the cure cycle in Figure 4. Residual transverse stress distributions are plotted against dimensionless thickness in Figure 15.

The plots indicate that the magnitude of the resin shrinkage significantly influences the parabolic stress distribution. The profile for v_{sh}^T=0% isolates the effect of non-uniform curing without resin shrinkage. It is interesting to note that for v_{sh}^T=1% the laminate is essentially stress free. In this case the processing strains due to chemical shrinkage are effectively equal in magnitude but opposite in sign to the thermal expansion processing strains.

3.7 Unsymmetric Curing Effects

All simulations presented to this point exhibited symmetric curing about the mid-plane of the laminate. The processing histories imposed on the laminates induced either inside-to-outside or outside-to-inside curing patterns. Consequently, all residual stress profiles were shown to be symmetric about the laminate mid-plane. When the thermal history is unsymmetric, the resulting stress profiles will also be unsymmetric. The following example demonstrates the influence of unsymmetric curing on residual stress development.

Unidirectional glass/polyester laminates of 1.38, 2.54 and 3.39 cm thickness were subjected to unsymmetric boundary conditions. The autoclave temperature cure cycle illustrated in Figure 4 was prescribed on the bottom surface of the laminate. An insulated boundary condition was imposed on the top surface. A volumetric resin shrinkage of v_{sh}^T=6% was assumed. In these simulations, the cure sweeps from the bottom to the top surfaces. The resulting residual transverse stress distributions are illustrated in Figure 16. Similar gradients are predicted for longitudinal stress distributions. Note that the stress profiles are self-equilibrating. It is interesting to contrast the magnitude of the peak transverse stress in the 2.54 cm laminate presented here to that which developed in the symmetrically cured laminate presented in Figure 11. The symmetric curing

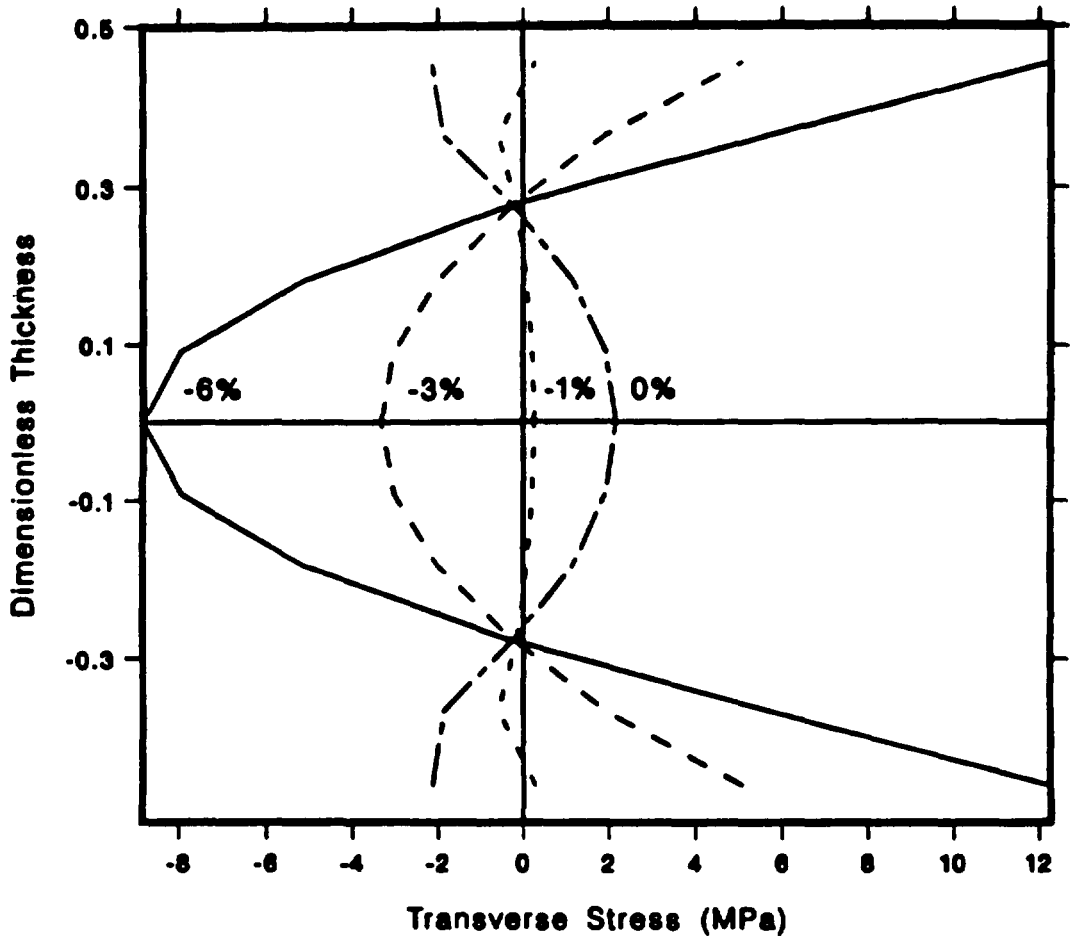

Figure 15: Resin shrinkage effects on residual in-plane transverse stress distributions in glass/polyester laminates (ℓ = 2.54 cm).

process resulted in transverse stresses ranging between -8.5 and 12.0 MPa while the unsymmetric curing process reduced stresses substantially (-2.0 and 2.0 MPa). This result is not surprising since the unsymmetric cure induces warpage in the laminate, reducing the magnitude of the in-plane residual stress.

3.8 Stacking Sequence Effects

The parametric studies presented to this point have focused on the unidirectional laminate configuration. This enabled the mechanisms of spatial solidification to be isolated, without the influence of the traditionally recognized stacking sequence effects. In the following examples, the influence of processing on stress development in [0/90] glass/polyester cross-ply laminates is quantified.

In the first example, a 2.54 cm laminate of [0/90] symmetric construction with 8 repeating units, ($[0/90]_{8s}$), was cured symmetrically according to the glass/polyester cure cycle with v_{sh}^{T}=6.0% (see Figure 4). The resulting tranverse stress distributions are shown in Figure 17. Such stress profiles are similar to what would be predicted by traditional laminated plate theory analysis that assumes a stress-free temperature. In this simulation, spatial solidification is present but negligible and one concludes that stacking sequence effects dominate.

In thicker laminates, however, spatial solidification cannot be neglected. Consider the resulting stress profiles in symmetric $[0/90]_{ns}$ laminates with n=8, 16 and 24 (corresponding to total laminate thicknesses of 2.54, 5.08 and 7.62 cm, respectively) shown in Figure 18. The profiles represent the envelope of peak normal stresses in the 0° or 90° plies through the laminate thickness. The stresses are discontinuous across ply interfaces and are equal and opposite in magnitude. Processing is shown to substantially increase the stress gradient with increasing laminate thickness. In contrast to the 2.54 cm laminate, the process-induced stress in the thicker laminates exhibit significant gradients through the thickness that are also much greater in magnitude in comparison with the traditional stacking sequence stress. This result further illustrates the significant influence the processing history has on stress development in thick-section thermosets, even for laminates of arbitrary stacking sequence.

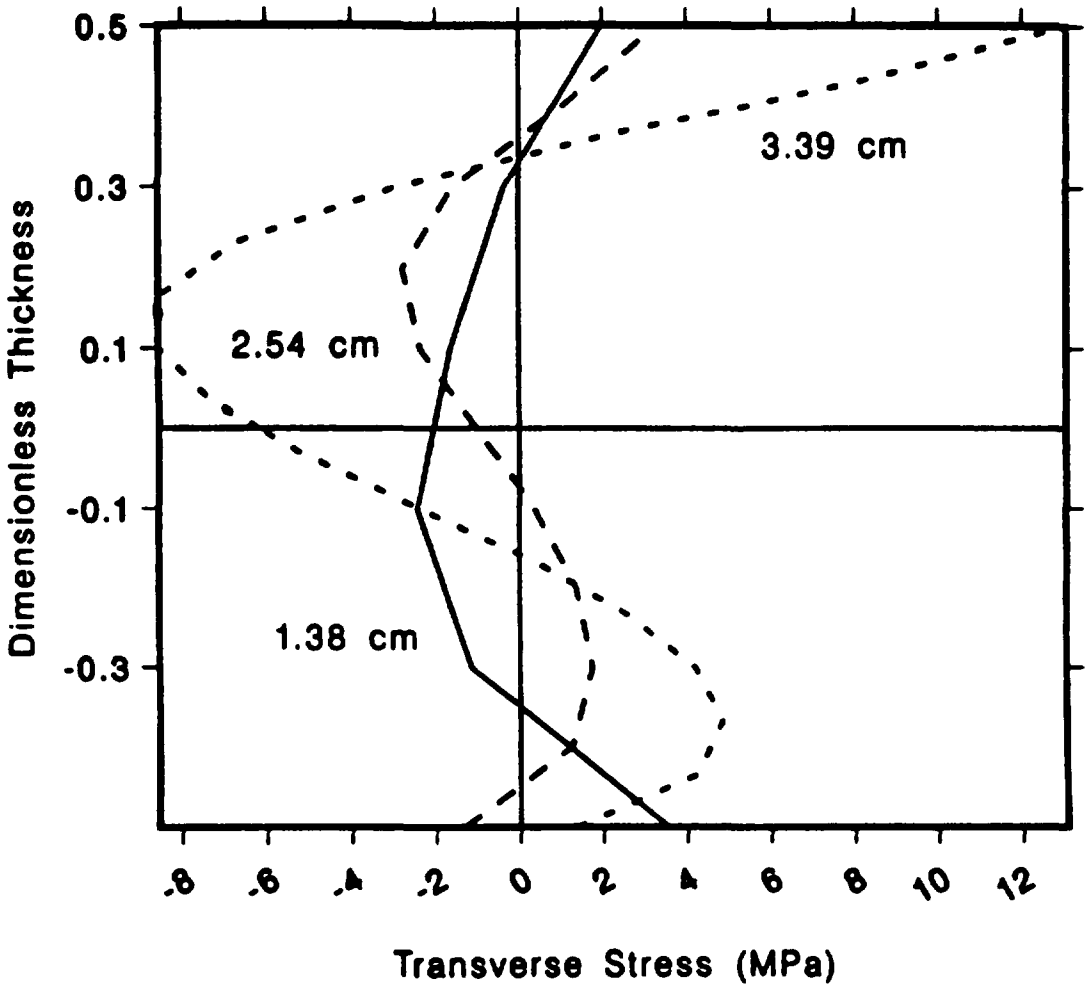

Figure 16: Influence of unsymmetric curing on transverse residual stress profiles in glass/polyester laminates.

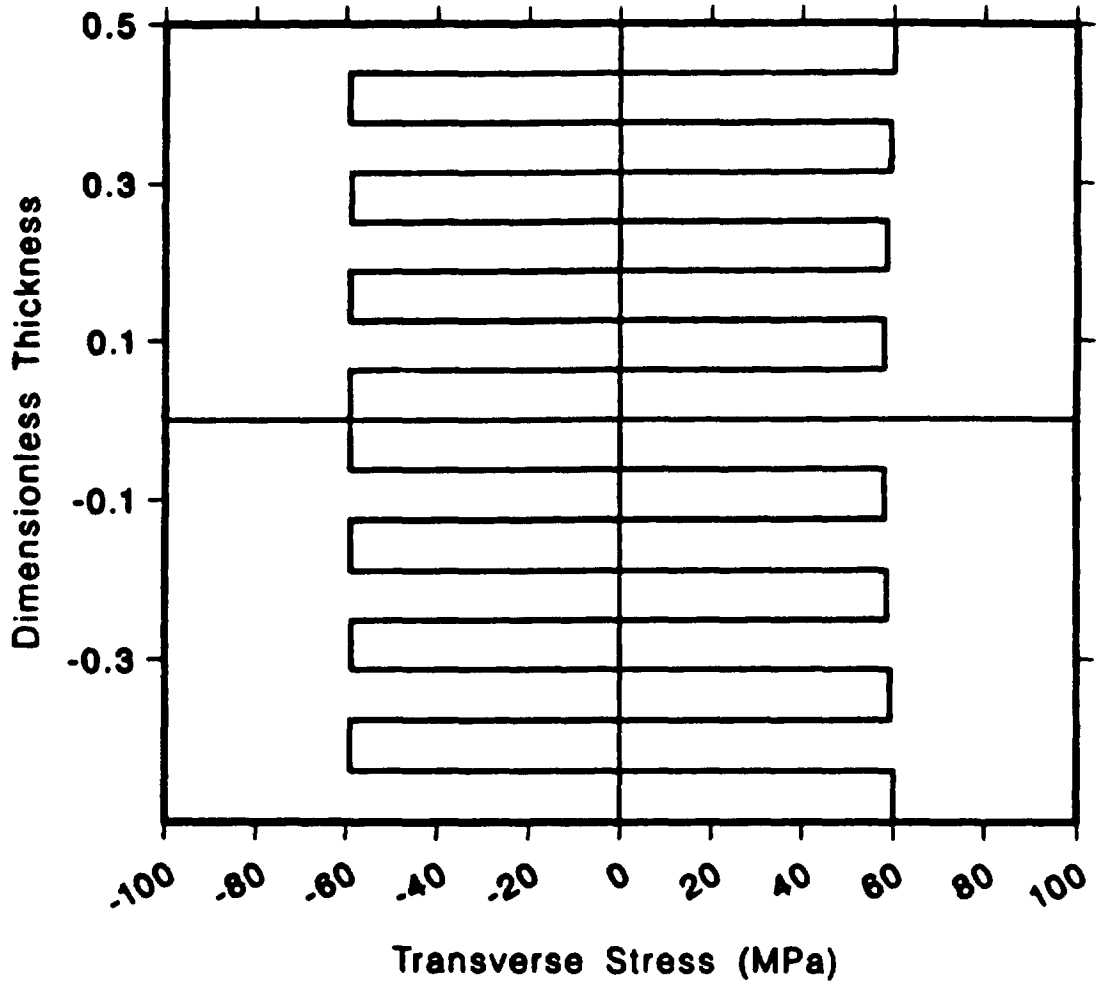

Figure 17: Transverse residual stresses in a $[0/90]_{8s}$ laminate.

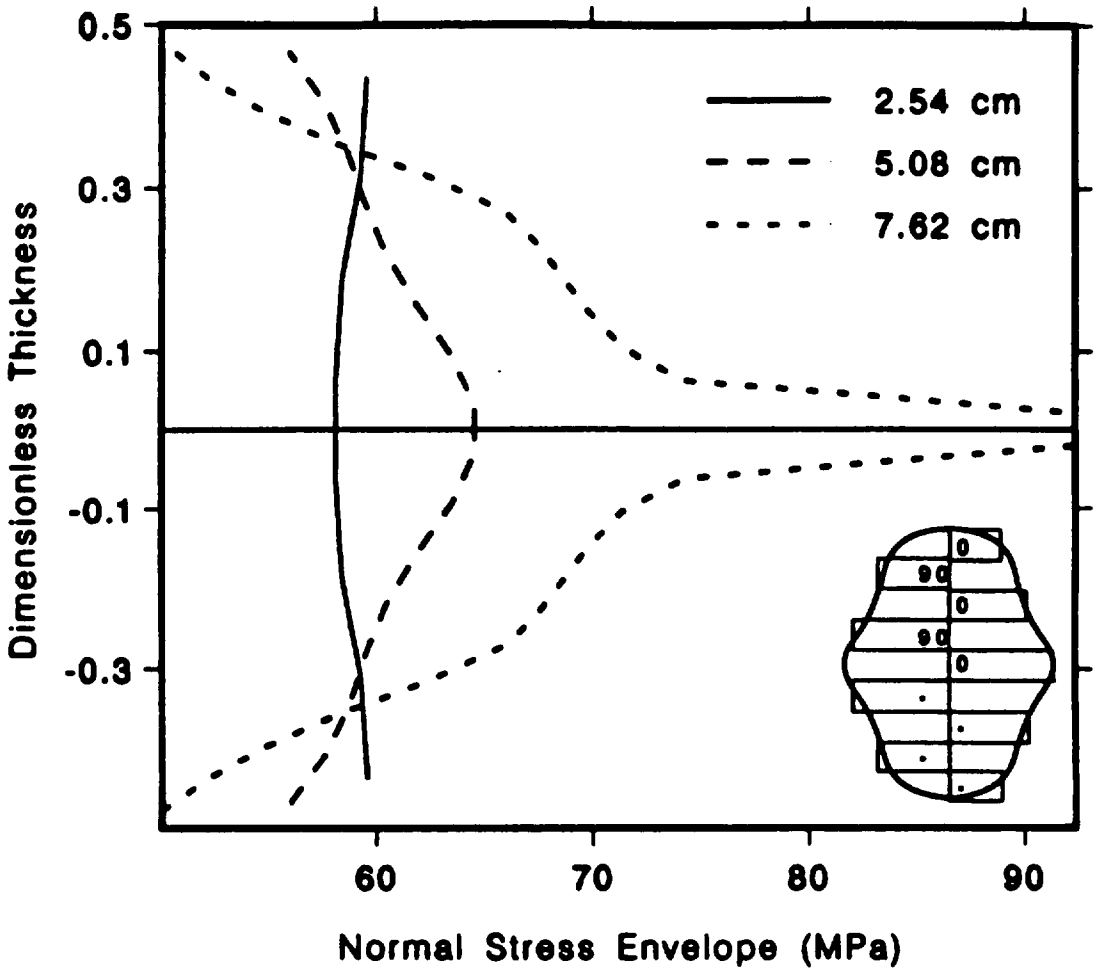

Figure 18: Normal residual stress envelopes in $[0/90]_{ns}$ laminates.

3.9 Stress-Free Temperature

Traditional residual stress predictions are based on a uniform stress-free temperature, commonly assumed to be the cure temperature. The uniform temperature drop to the operating temperature defines the temperature difference used to compute residual stresses. In the following example, the influence of resin shrinkage on the assumed stress-free temperature of a $[0/90]_s$ glass/polyester laminate is quantified.

The laminate thickness is chosen sufficiently thin to minimize temperature and degree of cure gradients during processing. In this case, stacking sequence is the dominant source of residual stress. The autoclave cure cycle is defined in Figure 4. Ply stresses are predicted for volumetric resin shrinkages between 0 and 6%. An equivalent stress-free temperature is defined from our predictions for comparison with the traditional methodology based on the assumption that ΔT=-106°C (the difference between ambient and the cure temperature). A dimensionless stress-free temperature difference is defined as the ratio of the predicted to the assumed temperature change. In Figure 19, dimensionless stress-free temperature is plotted against the volumetric resin shrinkage. Only for a volumetric shrinkage of 1% is the traditional assumption valid (ΔT=-106°C). The results demonstrate the significant influence that resin shrinkage can have on the assumed stress-free temperature, and thus the magnitude of the resulting residual stress distributions.

Another point worth noting is that in our simulation, the evolution of stress throughout the curing process is predicted and therefore no stress-free temperature assumption is required. Furthermore, the severe gradients in temperature and degree of cure that were shown to develop in thick laminates suggest that the traditional approach is not appropriate. This is apparent from the fact that significant residual stresses were shown to develop in thick unidirectional laminates. Recall that the traditional analysis predicts that unidirectional laminates are stress free. Therefore, the traditional residual stress analyses are not appropriate for thick-section laminates in general. The appropriateness of the assumption depends on many factors such as laminate thickness, resin shrinkage and the processing history.

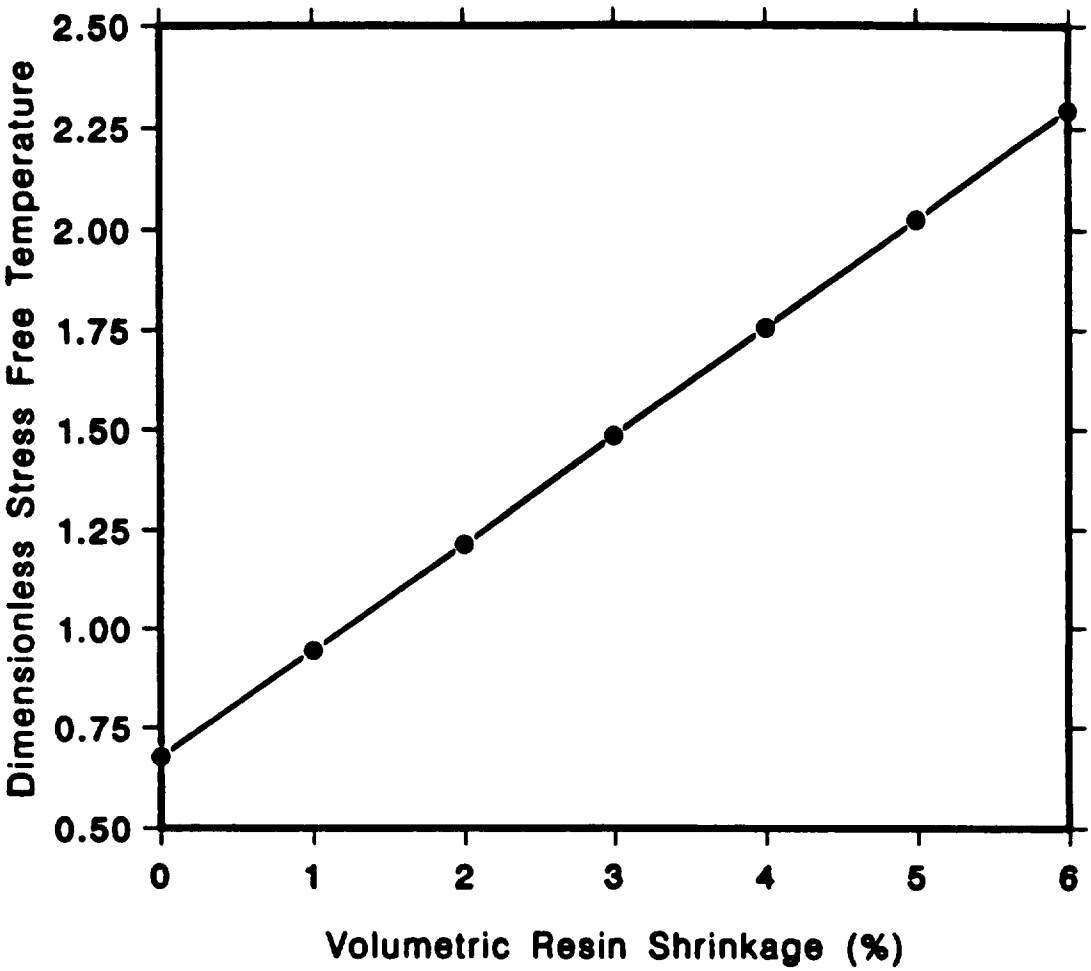

Figure 19: Influence of resin shrinkage on dimensionless stress-free temperature.

4 Conclusions

A fundamental study of process-induced stress and deformation in thick-section thermosetting composite laminates was presented. A methodology was proposed for predicting residual stress development during the curing process that does not require a stress-free temperature to be assumed. A one-dimensional cure simulation analysis was coupled to an incremental laminated plate theory model to study the relationships between complex gradients in temperature and degree of cure, and process-induced residual stress and deformation.

Material models were proposed to describe the mechanical properties, thermal and chemical strains of the thermoset resin during cure. The material models were incorporated into a micromechanics model to predict the effective mechanical properties and process-induced strains of the composite during cure. Thermal expansion and cure shrinkage contribute to changes in material specific volume and were shown to represent important sources of internal loading included in the analysis.

Temperature and degree of cure gradients that develop during the curing process induce mechanical property and process-induced strain gradients in the composite laminate. These gradients represent important mechanisms that contribute to stress and deformation development not previously considered in traditional residual stress analyses of laminated composites. Model predictions of cure dependent epoxy modulus and curvature in unsymmetric graphite/epoxy laminates were found to be in good agreement with experimental data presented in previously published literature.

The effects of processing history (autoclave temperature cure cycle), laminate thickness, resin cure shrinkage and laminate stacking sequence on the evolution of process-induced stress and deformation in thick-section glass/polyester and graphite/epoxy laminates during cure were quantified. Processing of unidirectional laminates was investigated to provide fundamental insight into the important mechanisms governing residual stress development during cure. While traditional sources of residual stress associated with laminate stacking sequence predict that unidirectional laminates are stress free, our results clearly indicate the potential for significant process-induced stress development in thick thermoset laminates.

Residual stresses were shown, in general, to increase with increasing laminate thickness, autoclave temperature ramp and resin shrinkage. Unsymmetric curing was shown to significantly reduce residual stress in comparison with a symmetric curing process. Spatial solidification and stacking sequence effects were found to be equally important in thick-section cross-ply laminates. Furthermore, the results indicated that the assumption of a stress-free temperature for residual stress predictions is not appropriate for thick-sections in general.

The present study has demonstrated fundamental mechanisms that contribute to residual stress development that have not been previously considered in traditional residual stress analyses of laminated composites. The significant magnitude of process-induced residual stress identified in this work substantiates the prevalent concerns associated with processing difficulties of thick thermosetting laminates, such as delaminations and matrix cracking. The results clearly indicate that the mechanics and performance of thick-section thermoset laminates are strongly dependent on processing history.

References

[1] Kau, H. and Petrusha, L.A. Dimensional stability and property gradients in thick smc sections. Technical Report GMR-6359, General Motors Research Laboratories, Warren Michigan, 1988.

[2] Kays, A.O. Exploratory development on processing science of thick section composites. Technical Report AFWAL-TR-85-4090, Air Force Wright Aeronautical Laboratories, Wright Patterson AFB, Ohio, 1985.

[3] Hahn, H.T. and Pagano, N.J. Curing stresses in composite laminates. *Journal of Composite Materials*, 9:91–105, 1975.

[4] Hahn, H.T. Residual stresses in polymer matrix composite laminates. *Journal of Composite Materials*, 10:266–277, 1976.

[5] Griffin, O.H. Three-dimensional curing stresses in symmetric cross-ply laminates with temperature-dependent properties. *Journal of Composite Materials*, 17:449–463, 1983.

[6] Stango, R.J. and Wang, S.S. Process-induced residual thermal stresses in advanced fiber-reinforced composite laminates. *Journal of Engineering for Industry*, 106:48–54, 1984.

[7] Pusatcioglu, S.Y., Hassler, J.C., Frickle, A.L., and McGee, Jr., H.A. Effect of temperature gradients on cure and stress gradients in thick thermoset castings. *Journal of Applied Polymer Science*, 25:381–393, 1980.

[8] Levitsky, M. and Shaffer, B.W. The approximation of temperature distributions in homogeneous exothermic reactions. *The Chemical Engineering Journal*, 5:235–242, 1973.

[9] Bogetti, T.A. and Gillespie, Jr., J.W. Two-dimensional cure simulation of thick thermosetting composites. *Journal of Composite Materials*, 1990. (accepted for publication).

[10] Bogetti, T.A. and Gillespie, Jr., J. W. Process-induced stress and deformation in thick-section thermosetting composite laminates. In *21st SAMPE Technical Conference*, Atlantic City, N.J., September, 1989.

[11] Bogetti, T.A. and Gillespie, Jr., J. W. Residual stress and deformation in thick laminate composites undergoing chemical hardening and shrinkage. In *SPI Composite Institute's 45th Annual Conference Proceedings*, Washington, D.C., February 12-15, 1990.

[12] Martin, L.P., Bogetti, T.A., and Gillespie, Jr., J. W. Influence of cure shrinkage on process-induced stress and deformation in thick thermosetting composites. In *5th Technical Conference of the American Society for Composites*, East Lansing Michigan, June 11-14, 1990.

[13] Bogetti, T.A. *Process-Induced Stress and Deformation in Thick-Section Thermosetting Composites.* PhD thesis, Department of Mechanical Engineering, University of Delaware, 1989.

[14] Lee, E.H., Rogers, T.G., and Woo, T.C. Residual stresses in a glass plate cooled symmetrically from both surfaces. *Journal of The American Ceramic Society*, 48:480–487, 1965.

[15] Tackels, G. and Crochet, M.J. Thermal stresses during annealing of a glass ribbon. *Rheologica Acta*, 12:330–336, 1973.

[16] Crochet, M.J., De Bast, J., Gilard, P., and Tackels, G. Experimental study of stress relaxation during annealing. *Journal of Noncrystalline Solids*, 14:242–254, 1974.

[17] Crochet, M.J. and Denayer, A. Transient and residual thermoviscoelastic stresses in glass. *Journal of Applied Mechanics*, 47:254–260, 1980.

[18] Muki, R. and Sternberg, E. On transient thermal stresses in viscoelastic materials with temperature dependent properties. *Journal of Applied Mechanics*, 28:193–207, 1961.

[19] Maneschy, C., Miyano, Y., Shimbo, M., and Woo, T.C. Residual-stress analysis of an epoxy plate subjected to rapid cooling on both surfaces. *Experimental Mechanics*, 26:306–312, 1986.

[20] Chapman, T.J., Gillespie, Jr., J.W., Pipes, R.B., Manson, J-A.E., and Serefis, J.C. Prediction of process-induced residual stresses in thermoplastic composites. *Journal of Composite Materials*, in press.

[21] Levitsky, M. and Shaffer, B.W. Thermal stresses in chemically hardening elastic media with application to the molding process. *Journal of Applied Mechanics*, 41:647–651, 1974.

[22] Shaffer, B.W. and Levitsky, M. Thermoelastic constitutive equations for chemically hardening materials. *Journal of Applied Mechanics*, 41:652–657, 1974.

[23] Levitsky, M. and Shaffer, B.W. Residual thermal stresses in a solid sphere cast from a thermosetting material. *Journal of Applied Mechanics*, 42:651–655, 1975.

[24] Boriek, A.M., Akin, J.E., and Armeniades, C.D. Setting stress distribution in particle reinforced polymer composites. *Journal of Composite Materials*, 22:986–1002, October 1988.

[25] Loos, A.C. and Springer, G.S. Curing of graphite/epoxy composites. Technical Report AFWAL-TR-83-4040, Air Force Wright Aeronautical Laboratories, Wright Patterson AFB, Ohio, 1983.

[26] Loos, A. C. and Springer, G. S. Curing of epoxy matrix composites. *Journal of Composite Materials*, 17:135–169, 1983.

[27] Adams, D.C. Cure behavior of unsaturated polyester resin composites. Technical Report CCM-88-16, Center for Composite Materials, University of Delaware, Newark, Delaware, 1988.

[28] Barakat, H.Z. and Clark, J.A. On the solution of the diffusion equations by numerical methods. *Journal of Heat Transfer*, 88:421–427, 1966.

[29] Dillman, S.H. and Seferis, J.C. Kinetic viscoelasticity for the dynamic mechanical properties of polymer systems. *Journal of Macromolecular Science-Chemistry*, 24, 1987.

[30] McGee, S. H. Curing of Particulate Filled Composites. *Polymer Engineering and Science*, 22:484, 1982.

[31] COMPCAL; Composite Calculations. Users manual. Technical Report Technomic Publishing Co., Inc., Lancaster, PA, Center for Composite Manufacturing Science and Engineering, 1987.

[32] Whitney, J.M. and McCullough, R.L. Analytical design methods. In *Composites Design Guide*, Center for Composite Materials, University of Delaware, 1980. Center for Composite Materials.

[33] Vinson, J.R. and Sierakowski. *The Behavior of Structures Composed of Composite Materials.* Martinus Nijhoff Publishers, Dordrecht, Netherlands, 1986.

[34] Whitney, J.M. *Structural Analysis of Laminated Anisotropic Plates.* Technomic Publishing, Lancaster, PA, 1987.

[35] Bogetti, T.A. Predicting nonlinear behavior in laminated composites. Master's thesis, Department of Mechanical Engineering, University of Delaware, 1986.

[36] Hahn, H.T. and Kim, K.S. Residual stress development during processing of graphite/epoxy composites. *Composites Science and Technology*, 1989. (submitted for publication).

[37] Hill, R. Theory of Mechanical Properties of Fibre-Strengthened Materials: III. Self-Consistent Model. *Journal of Mechanics and Physics of Solids*, 13:189, 1965.

A Continuous Fiber Micromechanics Model

The doubly embedded self-consistent field model approach, based on the work of Hill [37], offers a more realistic approximation of the effective lamina properties than mechanics of materials models based on the uniform stress or strain assumption. The model also offers mathematically tractable closed-form expressions for the effective lamina mechanical properties and expansion strains. Theoretical background of the model is presented in greater detail elsewhere [32].

In the equations presented below, the subscripts 1, 2, and 3 refer to the directions in the principle coordinate system of the lamina. Subscripts m and f correspond to the matrix (resin) and fiber properties, respectively. Fiber volume fraction of the lamina is denoted as v_f and k is the isotropic plane strain bulk modulus defined by

$$k = \frac{E}{2(1-\nu-2\nu^2)} \tag{24}$$

A.1 Engineering Constants

The following equations define the transversely isotropic engineering constants of the lamina. The longitudinal Young's modulus:

$$E_1 = E_{1f}v_f + E_{1m}(1-v_f) + \left[\frac{4(\nu_{12m}-\nu_{12f}^2)k_f k_m G_{23m}(1-v_f)v_f}{(k_f+G_{23m})k_m + (k_f-k_m)G_{23m}v_f}\right] \tag{25}$$

The major Poisson's ratio:

$$\nu_{12} = \nu_{13} = \nu_{12f}v_f + \nu_{12m}(1-v_f) + \left[\frac{(\nu_{12m}-\nu_{12f})(k_m-k_f)G_{23m}(1-v_f)v_f}{(k_f+G_{23m})k_m + (k_f-k_m)G_{23m}v_f}\right] \tag{26}$$

The in-plane shear modulus:

$$G_{12} = G_{13} = G_{12m}\left[\frac{(G_{12f}+G_{12m})+(G_{12f}-G_{12m})v_f}{(G_{12f}+G_{12m})-(G_{12f}-G_{12m})v_f}\right] \tag{27}$$

The transverse shear modulus:

$$G_{23} = \frac{G_{23m}[k_m(G_{23m}+G_{23f})+2G_{23f}G_{23m}+k_m(G_{23f}-G_{23m})v_f]}{k_m(G_{23m}+G_{23f})+2G_{23f}G_{23m}-(k_m+2G_{23m})(G_{23f}-G_{23m})v_f} \tag{28}$$

The transverse Young's modulus:

$$E_2 = E_3 = \frac{1}{(1/4k_T) + (1/4G_{23}) + (\nu_{12}^2/E_1)} \tag{29}$$

where k_T is the effective plane strain bulk modulus of the composite given by

$$k_T = \frac{(k_f + G_{23m})k_m + (k_f - k_m)G_{23m}v_f}{(k_f + G_{23m}) - (k_f - k_m)v_f} \tag{30}$$

The transverse Poisson's ratio:

$$\nu_{23} = \frac{2E_1k_T - E_1E_2 - 4\nu_{12}^2k_TE_2}{2E_1k_T} \tag{31}$$

A.2 Expansional Strains

Expansional strain expressions are used to evaluate the in-plane chemical shrinkage strains and the effective coefficients of thermal expansion of the lamina ($\alpha_1 = \epsilon_1$ and $\alpha_2 = \epsilon_2$). The following equations define the transversely isotropic expansional strains of the lamina. The longitudinal direction expansional strain:

$$\epsilon_1 = \frac{\epsilon_{1f}E_{1f}v_f + \epsilon_{1m}E_{1m}(1 - v_f)}{E_{1f}v_f + E_{1m}(1 - v_f)} \tag{32}$$

The transverse direction expansional strain:

$$\epsilon_2 = \epsilon_3 = (\epsilon_{2f} + \nu_{12f}\epsilon_{1f})v_f + (\epsilon_{2m} + \nu_{12m}\epsilon_{1m})(1 - v_f) - [\nu_{12f}v_f + \nu_{12m}(1 - v_f)]\left[\frac{\epsilon_{1f}E_{1f}v_f + \epsilon_{1m}E_{1m}(1-v_f)}{E_{1f}v_f + E_{1m}(1-v_f)}\right] \tag{33}$$

No of Copies	Organization
2	Administrator Defense Technical Info Center ATTN: DTIC-DDA Cameron Station Alexandria, VA 22304-6145
1	HQDA (SARD-TR) WASH DC 20310-0001
1	Commander US Army Materiel Command ATTN: AMCDRA-ST 5001 Eisenhower Avenue Alexandria, VA 22333-0001
1	Commander US Army Laboratory Command ATTN: AMSLC-DL Adelphi, MD 20783-1145
2	Commander US Army, ARDEC ATTN: SMCAR-IMI-I Picatinny Arsenal, NJ 07806-5000
2	Commander US Army, ARDEC ATTN: SMCAR-TDC Picatinny Arsenal, NJ 07806-5000
1	Director Benet Weapons Laboratory US Army, ARDEC ATTN: SMCAR-CCB-TL Watervliet, NY 12189-4050
1	Commander US Army Armament, Munitions and Chemical Command ATTN: SMCAR-ESP-L Rock Island, IL 61299-5000
1	Commander US Army Aviation Systems Command ATTN: AMSAV-DACL 4300 Goodfellow Blvd. St. Louis, MO 63120-1798

No of Copies	Organization
1	Director US Army Aviation Research and Technology Activity ATTN: SAVRT-R (Library) M/S 219-3 Ames Research Center Moffett Field, CA 94035-1000
1	Commander US Army Missile Command ATTN: AMSMI-RD-CS-R (DOC) Redstone Arsenal, AL 35898-5010
1	Commander US Army Tank-Automotive Command ATTN: AMSTA-TSL (Technical Library) Warren, MI 48397-5000
1	Director US Army TRADOC Analysis Command ATTN: ATAA-SL White Sands Missile Range, NM 88002-5502
(Class. only)1	Commandant US Army Infantry School ATTN: ATSH-CD (Security Mgr.) Fort Benning, GA 31905-5660
(Unclass. only)1	Commandant US Army Infantry School ATTN: ATSH-CD-CSO-OR Fort Benning, GA 31905-5660
1	Air Force Armament Laboratory ATTN: AFATL/DLODL Eglin AFB, FL 32542-5000
	Aberdeen Proving Ground
2	Dir, USAMSAA ATTN: AMXSY-D AMXSY-MP, H. Cohen
1	Cdr, USATECOM ATTN: AMSTE-TD
3	Cdr, CRDEC, AMCCOM ATTN: SMCCR-RSP-A SMCCR-MU SMCCR-MSI
1	Dir, VLAMO ATTN: AMSLC-VL-D

No. of Copies	Organization
1	Oak Ridge National Laboratory Applied Technology Division ATTN: Ray Garvey P.O. Box 2003, NS-7294 Oak Ridge, TN 37831-7294
3	DTRC ATTN: R. Rockwell W. Phyillaier J. Corrado Bethesda, MD 20084-5000
1	Naval Research Laboratory ATTN: I. Wolock 4555 Overlook Avenue, Southwest Washington, DC 20375-5000
2	Director Benet Weapons Laboratory US Army, ARDEC ATTN: L. Johnson G. De Andrea Watervliet, NY 12189-4050
6	Lawrence Livermore National Laboratory ATTN: R. M. Christensen L. Chiao S. De Teresa F. Magness W. Feng J. Lepper P.O. Box 808 Livermore, CA 94550
5	Sandia National Laboratory, Livermore Applied Mechanics Department Engineer Design Division ATTN: C. W. Robinson B. Benedetti W. W. Kawahara P. Neilman D. Barnman Livermore, CA 94550

No. of Copies	Organization
5	U.S. Army Materials Technology Laboratory ATTN: SLCMT-MEC, B. Halpin (2) W. Haskell D. Granville S. Walsh Watertown, MA 02172-0001
1	University of Utah ATTN: Professor S. Swanson Salt Lake City, UT 84112
1	Virginia Polytechnic Institute & State University ATTN: Professor M. Hyer Blackburg, VA 24061-0214
1	The Pennsylvania State University ATTN: Professor T. Hahn 227 Hammond Building University Park, PA 16802
2	University of Illinois ATTN: Professor S. S. Wang 104 S. Wright Street Urbana, IL 61801
1	Stanford University ATTN: Dr. Steve Tsai Palo Alto, CA 94301
4	University of Delaware Center of Composite Materials Department of Mechanical Engineering ATTN: John W. Gillespie, Jr. Neward, DE 19716
2	Wright Research & Development Center ATTN: J. Whitney F. Abrams Dayton, OH 45433
2	Battelle PNL ATTN: M. Smith P.O. Box 999 Richland, WA 99352

No. of Copies	Organization
2	Olin Corporation ATTN: H. Parkinson D. Marlow 707 Berkshire Street East Alton, IL 62024-1174
3	Honeywell, Inc. ATTN: G. Campbell G. Stelmasic J. Bode 5640 Smitana Drive Minnetonka, MN 55343
2	FMC Corporation ATTN: Eric Weerth Manager, Advance Structures and Materials Dept 1105 Coleman Avenue, Box 1201 San Jose, CA 95108
2	ARDEC CCAC ATTN: S. Mursalli J. Hederich Picatinny Arsenal, NJ 07806-5000
2	PM-TMAS Picatinny Arsenal, NJ 07806-5000
2	DARPA ATTN: J. Kelly 1400 Wilson Blvd Arlington, VA 22209

No. of Copies Organization

INTENTIONALLY LEFT BLANK.

USER EVALUATION SHEET/CHANGE OF ADDRESS

This Laboratory undertakes a continuing effort to improve the quality of the reports it publishes. Your comments/answers to the items/questions below will aid us in our efforts.

1. BRL Report Number BRL-TR-3182 Date of Report DECEMBER 1990

2. Date Report Received _____

3. Does this report satisfy a need? (Comment on purpose, related project, or other area of interest for which the report will be used.) _____

4. Specifically, how is the report being used? (Information source, design data, procedure, source of ideas, etc.) _____

5. Has the information in this report led to any quantitative savings as far as man-hours or dollars saved, operating costs avoided, or efficiencies achieved, etc? If so, please elaborate. _____

6. General Comments. What do you think should be changed to improve future reports? (Indicate changes to organization, technical content, format, etc.) _____

CURRENT ADDRESS

_____
Name

_____
Organization

_____
Address

_____
City, State, Zip Code

7. If indicating a Change of Address or Address Correction, please provide the New or Correct Address in Block 6 above and the Old or Incorrect address below.

OLD ADDRESS

_____
Name

_____
Organization

_____
Address

_____
City, State, Zip Code

(Remove this sheet, fold as indicated, staple or tape closed, and mail.)

---FOLD HERE---

DEPARTMENT OF THE ARMY
Director
U.S. Army Ballistic Research Laboratory
ATTN: SLCBR-DD-T
Aberdeen Proving Ground, MD 21[illegible]-5066
OFFICIAL BUSINESS

NO POSTAGE
NECESSARY
IF MAILED
IN THE
UNITED STATES

BUSINESS REPLY MAIL
FIRST CLASS PERMIT No 0001, APG, MD

POSTAGE WILL BE PAID BY ADDRESSEE

Director
U.S. Army Ballistic Research Laboratory
ATTN: SLCBR-DD-T
Aberdeen Proving Ground, MD 21005-9989

---FOLD HERE---